

# Pattern formation in chemically reactive, phase-separating systems

Coleman Broaddus

November 4, 2013



# Contents

<b>1</b>	<b>Introduction</b>	<b>7</b>
<b>2</b>	<b>General features of two phase systems</b>	<b>9</b>
2.1	Physical description of binary fluids . . . . .	9
2.2	Equilibrium . . . . .	11
2.3	Nonequilibrium dynamics . . . . .	15
2.4	Chemical reactions . . . . .	17
<b>3</b>	<b>Lattice model</b>	<b>19</b>
3.1	Definition of lattice model . . . . .	19
3.2	Equilibrium properties . . . . .	20
3.2.1	Equilibrium statistical mechanics . . . . .	20
3.2.2	Metropolis algorithm for computing ensemble averages . . . . .	21
3.2.3	Relationship to continuous description . . . . .	22
3.3	Nonequilibrium dynamics via Kawasaki exchange . . . . .	26
3.4	Chemical reactions on the lattice . . . . .	27
3.4.1	First order reactions . . . . .	27
3.4.2	Autocatalytic reactions . . . . .	29
<b>4</b>	<b>Stationary state morphology</b>	<b>31</b>
4.1	Passive system . . . . .	31
4.2	First Order Reactions . . . . .	33
4.3	Autocatalytic Reactions . . . . .	36
<b>5</b>	<b>Coarsening Dynamics</b>	<b>43</b>
5.1	Passive systems . . . . .	43
5.2	First order reactions . . . . .	47
5.3	Autocatalytic reactions . . . . .	48
<b>6</b>	<b>Summary</b>	<b>51</b>
6.1	Steady state behavior . . . . .	51
6.2	Coarsening dynamics . . . . .	52
6.3	Outlook . . . . .	52



# Acknowledgements

Much of the credit for this work must be given to David Zwicker, who served as my immediate supervisor and mentor for the duration of this Thesis. David was extremely generous with his time and attention, and his deep knowledge on the topic of phase separation was invaluable. Additionally, sincere thanks must be given to our department head Frank Julicher, who can be credited for initially proposing this project which proved to be well balanced between the pedagogical and the original. I would like to thank Hans-Georg Braun for agreeing to the role of supervisor, as well as for his interest in our project and a fruitful discussion. My gratitude to the Max Planck Institute for the Physics of Complex Systems for providing a home from which this work could be performed. Lastly I would like to thank the Biotechnology Center TU Dresden for organization and support, in particular Anne Chesneau, Martina Flockezi and our program head Jochen Guck.



# Chapter 1

## Introduction

Phases are regions within a system where the physical properties of the material are homogeneous. When a single system contains multiple phases at the same time which can freely exchange material these phases are said to *coexist*. A common example of a liquid system with coexisting phases is that of oil and vinegar. At room temperature the oil and vinegar resting in the same dish are separated into clearly defined regions. However, with vigorous stirring we can force the oil and vinegar to mix into one homogeneous blob. Left untouched, over time the oil and vinegar will begin to separate from one another, a process called *demixing*, eventually reforming the two separate phases found in the unstirred system. The behavior is even more interesting when we acknowledge the relatively complex molecular makeup of each phase. Oils may contain many different types of lipids, proteins and waxes. Vinegar is a mixture of acetic acid, water and possibly other chemicals for flavor or color. Why does the system demix? How does the system know which kinds of molecules to group together? To answer these question we must explore the thermodynamics of phase separation.

The simplest examples of systems with coexisting phases are found in two-phase systems like oil and vinegar. Similar demixing behavior can be observed in many other physical systems. Classical examples are polymer solutions and metal alloys [2]. In alloys the phases may represent a mixture of atoms in different ratios on a crystal lattice. In polymer systems they may correspond to different fraction of polymers in a polymer-solvent mixture, or to different packing structures. [2]

While many systems exhibit interesting equilibrium phase behavior, we may also be interested in phase-separation as a dynamic process. The transitions from a perturbed, out of equilibrium state (the stirred system in the case of oil and vinegar) back to equilibrium involves the complex rearrangement of material. This development of a quantitative physical description of this transition is thus quite challenging.

Additionally, from a technological point the transient structures formed during this process may have more useful physical properties, so understanding and ultimately controlling or halting the phase separation process is of practical in-

terest.

Despite its difficulty, the dynamics of a two phase system which is undergoing a transition from the homogeneous to the phase-separated state is an old, and well studied problem [13]. This process in which initially well-mixed system develops small regions of different phase which grow and rearrange over time is known as *coarsening*. The growth law proposed by Lifshitz and Slyozov is a classical result in the study of coarsening dynamics and has been extensively studied. A phenomenological theory which describes the full spatial evolution of coarsening processes was given initially by Cahn and Hilliard [5]. Although their theory was used initially to explain the coarsening dynamics found in alloys [11], in recent years it has found a wide range of applications in seemingly unrelated systems from the migration of bacterial colonies [6] to the patterning of mussel beds [15].

Biological systems are of particular interest both because of their complexity and prevalence in nature, but also from the point of view of general pattern formation. In order to sustain life biological systems must maintain themselves in states far from equilibrium. Thus, much of what we know from equilibrium and near-equilibrium systems does not apply in the context of biological systems. However, this complexity also allows for a wide range of fundamentally new behavior.

More recently, the existence of liquid-like droplets of material have been discovered to coexist within the cytoplasm of cells [4]. Even more interesting is the discovery that biological systems are capable of using the physics of phase-separation to serve some biological function [12], and that

“liquid-liquid phase separation of the cytoplasm may be an important principle for the spatial organization of the cell.” - Lee *et al*

Actively driven chemical processes are a characteristic feature of life within cells. We find of particular interest the recent work by Zwicker *et al* which provides an example of a subcellular biological process combining liquid-liquid phase separation in the cytoplasm with actively driven chemical reactions. It is found that the nematode worm *Caenorhabditis elegans* uses specifically autocatalytic chemical reactions to tightly control the creation of centrosomes (large, subcellular structures) in time.

While demixing in phase-separating mixtures containing first order chemical reactions have been studied for a limited set of parameters, a thorough exploration of possible patterning behavior in such systems remains incomplete [14] [9] [8]. Additionally, possible morphologies resulting from autocatalytic reactions remains largely unexplored.

In this thesis we aim to modify a very general model for two-phase isotropic systems through the inclusion of both first-order and autocatalytic chemical reaction schemes. The temporal evolution spatial patterns is studied for a large set of systems of differing compositions, temperatures and reaction rates.

## Chapter 2

# General features of two phase systems

There is much that can be learned about two-phase systems without the need to develop a complex or specific molecular model. In this chapter we will introduce a minimal model capable of two-phase behavior as well as general analytical techniques which shall be used throughout this thesis.

We begin by developing the phenomenological description of these systems first introduced by Landau. Various limiting cases are analyzed and the conditions for the stability of the homogeneous, well-mixed, solution are identified. Lastly, we extend the model to include time dynamics and introduce a simple method for including chemical reactions.

### 2.1 Physical description of binary fluids

We are interested in phase separation in fluids, and while in general fluids contain long range interactions, like convective flow, for simplicity we restrict the set of systems to those composed solely of short range interactions causing diffusive motion and chemical reactions. Additionally, all systems are considered incompressible and with constant volume and external pressure.

We consider a model containing two molecular components, A and B, where the local amount of each component can be described in terms of its volume density, respectively  $\phi_A$  and  $\phi_B$ . We assert that together A and B fill space, i.e.  $\phi_A + \phi_B = 1$ , which implies that  $\phi_A$  and  $\phi_B$  are uniquely determined by their difference:  $\phi = \phi_A - \phi_B$ .  $\phi$  is a function of space and time.

The free energy of a system completely determines it's equilibrium morphology. In this section we introduce the Landau phenomenological free energy as a description of a two component fluid. Using this description we determine the conditions for one and two phase equilibrium states as well as an equation of motion for near-equilibrium systems.

The Landau free energy describes isotropic systems with a phenomenological term that assigns an energetic cost to spatial inhomogeneities. We assume *local equilibrium*, i.e. that the system can be treated as equilibrium on short length scales and over long times. The free energy can be derived by first assuming a functional form

$$F = \int_V f(\phi, \nabla\phi, T) d^d x , \quad (2.1)$$

where  $V$  is constant and  $f$  may depend on arbitrary powers of  $\phi$  and its spatial derivatives. Assuming that the derivatives of  $\phi$  are small, we take the gradient expansion of  $f$  up to second order, discarding higher order terms which scale rapidly with the characteristic length scale of the system. Keeping all the terms allowed by the symmetry group of an isotropic fluid in combination with either no flux or periodic boundary conditions leaves us with the following expression for the free energy, often called the Landau free energy [7]

$$F(\phi, T) = \int_V \left\{ f(\phi, T) + \frac{\kappa}{2} (\nabla\phi)^2 \right\} d^d x , \quad (2.2)$$

where  $\kappa \geq 0$ . Equilibrium is defined as the state where no net fluxes of material or energy exist. When gradients in the chemical potential  $\mu$  are sufficiently small the flux  $\mathbf{j}_\phi$  of  $\phi$  may be approximated as

$$\mathbf{j}_\phi = -m \nabla \mu , \quad (2.3)$$

where  $m$  is a proportionality factor called the *mobility* which for simplicity we assume to be independent of  $\phi$ . The chemical potential  $\mu$  is given by the variational derivative of  $F$

$$\mu = \frac{\delta F}{\delta \phi} . \quad (2.4)$$

Evaluating the functional derivative we see that the equilibrium state  $\phi(\mathbf{x})$  satisfies

$$\mu = \frac{\partial f}{\partial \phi} - \kappa \nabla^2 \phi = \text{const} , \quad (2.5)$$

while the average volume fraction

$$\Phi(t) \equiv \frac{1}{V} \int_V \phi(\mathbf{x}, t) d^d x , \quad (2.6)$$

simultaneously satisfies the material conservation law

$$\Phi(t) = \Phi_0 . \quad (2.7)$$

We note that (2.5) is almost always nonlinear and very often analytically intractable. In general the free energy density  $f(\phi, T)$  depends on the specific

mixture in question and may be an arbitrarily complex function. We can however analyze a simple, model free energy density, which accurately describes a large class of systems given a certain set of assumptions.

Assume first that we are interested in the behavior of the system near its critical point, where it undergoes a continuous phase transition at the temperature  $T_c$ . Next, we assume that the particles  $A$  and  $B$  are sufficiently similar in their self-interactions that the free energy density can be taken to exhibit  $\phi \leftrightarrow -\phi$  symmetry. This allows us to expand the free energy in an even power series of the form

$$f(\phi, T) = f_0 + a\phi^2 + b\phi^4 + O(\phi^6), \quad (2.8)$$

where both  $a$  and  $b$  can in principle depend on  $T$ . We know that  $b$  must be positive in order that forms of  $f$  exist with two stable minima. The simplest free energy density which satisfies these criteria is

$$f(\phi, T) = (T - T_c)\phi^2 + b\phi^4. \quad (2.9)$$

For all temperatures  $T \geq T_c$  the  $f$  contains a single minimum at  $\phi = 0$ . For temperatures  $T < T_c$   $f$  has two minima equally spaced about  $\phi = 0$  and is called a *double-well potential* (see figure 2.1).

## 2.2 Equilibrium

In “classical” equilibrium thermodynamics systems are considered homogeneous and thus gradient terms like those in (2.2) are not considered. We can regain a classical form from (2.2) by setting  $\kappa = 0$ . In this case, the equilibrium configuration is determined by the free energy density (2.9) and the average volume fraction (2.7). Inserting this free energy density into (2.5) results in

$$2(T - T_c)\phi + 4b\phi^3 - \kappa\nabla^2\phi = \text{const} , \quad (2.10)$$

which is a condition for equilibrium in a simple quartic free energy density model. When  $T > T_c$  the minimization (2.10) is accomplished by  $\phi(\mathbf{x}) = \Phi_0$ , a homogeneous field. The gradient squared term in this case is everywhere zero, and so the classical and Landau free energies have the same solution.

When  $T < T_c$  the free energy density takes the form of a double well potential. If the average volume fraction  $\Phi_0$  is in between the two minima of  $f$  the system will be able to lower its classical free energy by dividing its material into regions of differing phase. The local volume fraction in these regions are  $\phi_{m_-}$  and  $\phi_{m_+}$ , which are the values of  $\phi$  at the minima of  $f$ . Specifically,  $\Phi_0$  must satisfy

$$\phi_{m_-} < \Phi_0 < \phi_{m_+} \quad (2.11)$$

in order for a lower energy configuration to exist in the case  $\kappa = 0$ . When this condition is met the equilibrium configuration contains two coexisting phases.

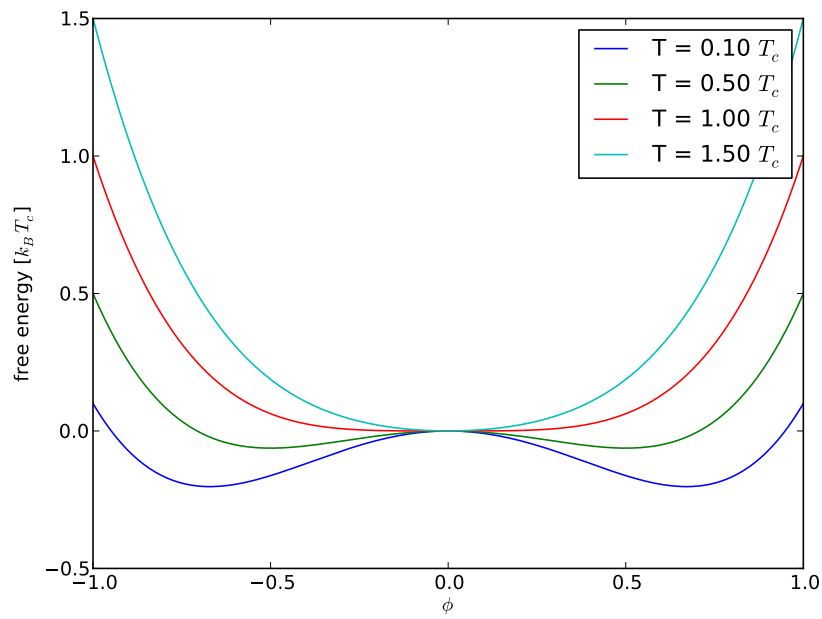


Figure 2.1: A double well potential forms as temperature is increased beyond  $T_c$ . Two minima allow the possibility of coexisting phases.

As  $f$  is an even function they are symmetric about zero, and we can refer to them simply as  $\pm\phi_m$ . We can solve for  $\pm\phi_m$  in terms of the free energy parameters

$$\pm\phi_m = \pm\sqrt{\frac{(T_c - T)}{2b}} \quad (2.12)$$

In figure 2.2 we show the phase space for the externally controlled parameters  $T$  and  $\Phi_0$  with the two-phase region shaded in blue. The line separating the one and two phase regions is called the *binodal*.

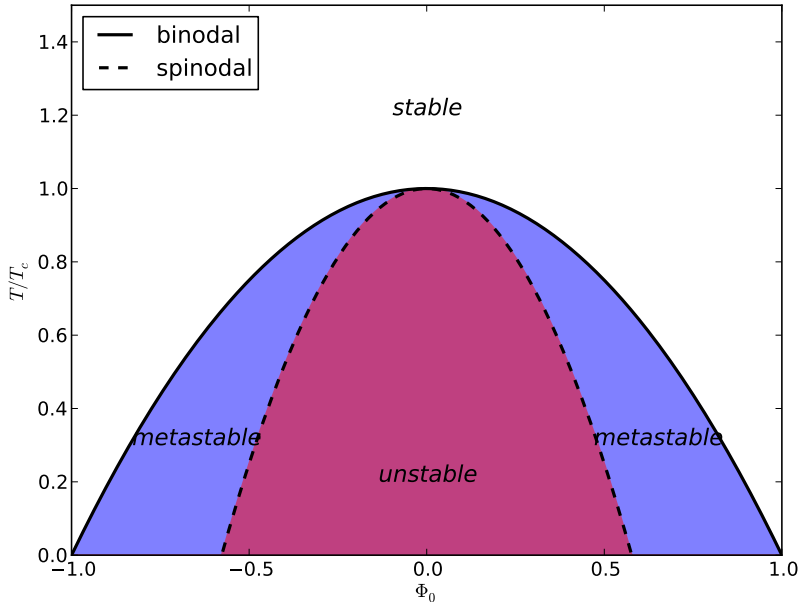


Figure 2.2: Phase portrait showing binodal and spinodal lines for free energy density  $f(\phi) = (T - T_c)\phi^2 + 1/2\phi^4$ . Above the binodal the equilibrium state has single, homogeneous phase. Beneath it the equilibrium state has coexisting phases. Beneath the spinodal a homogeneously prepared system is unstable and coarsens via spinodal decomposition. Between the spinodal and binodal a homogeneously prepared system is metastable and coarsens via nucleation and growth.

When we allow  $\kappa > 0$  in one dimensional systems of finite size the solutions to (2.10) and (2.7) take on the form

$$\phi(x) = \pm\phi_m \tanh\left(\sqrt{\frac{|T - T_c|}{2\kappa}}(x - x_0(\Phi_0))\right), \quad (2.13)$$

where  $x_0(\Phi_0)$  is parameter which adjusts the location of the interface in the system so as to satisfy (2.7) [16]. In this solution we see the formation of a single, continuous interface separating two largely homogeneous regions. The width of this interface is proportional to  $\sqrt{\kappa}$ . In the limit  $\kappa \rightarrow 0$  we regain the piecewise constant solution which satisfies a classical free energy. We contrast the set of solutions obtained in this limit with the much larger set obtained when one begins with a classical free energy, i.e. first taking  $\kappa \rightarrow 0$ , then solving for  $\phi(x)$ . The latter contains all piecewise constant functions  $\phi(x) \in \pm\phi_m$  which satisfy the global conservation constraint (2.7), which may contain arbitrarily many regions, each separated by an infinitely sharp interface. In figure 2.3 we show typical examples for the one and two-phase solutions, as well as showing the effect of  $\kappa$  on the shape of the interface.

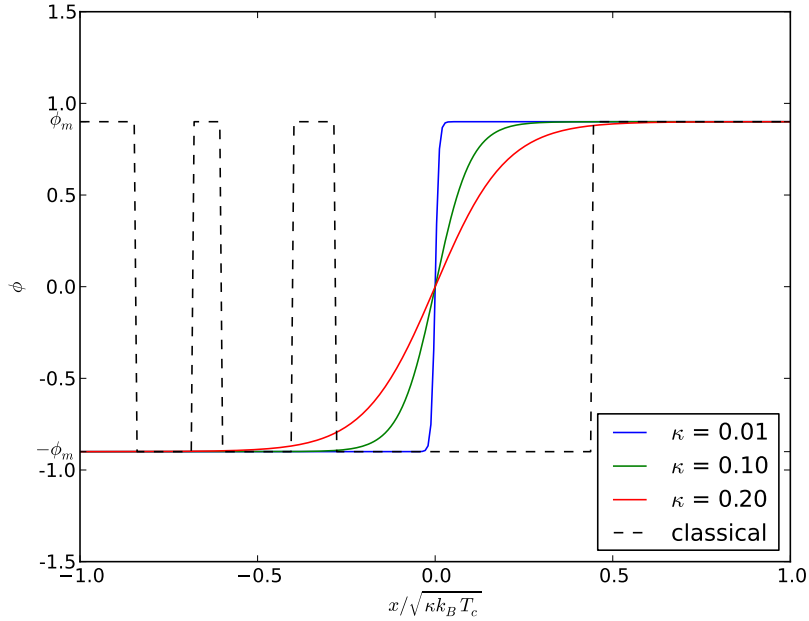


Figure 2.3: The tanh solution which minimizes the Landau free energy (2.2) is compared for various values of  $\kappa$ . Note that all solutions have the same average value  $\Phi_0$  and correspond to the same free energy density, giving fixed values for  $\pm\phi_m$ . An example piecewise constant solution to the classical free energy without gradient terms is shown for comparison (dashed black line).

The tanh solutions under the limit  $\kappa \rightarrow 0$  are contained within the larger set of classical solutions as the subset with *minimal interfacial area*. Area minimization is observed in real systems as a result of surface tension. The Landau free energy can be seen as introducing an effective surface tension between phases,

the strength of which is controlled by the parameter  $\kappa$ .

## 2.3 Nonequilibrium dynamics

If a system at equilibrium in the one-phase region of phase space is rapidly cooled and brought into the two-phase region it will undergo a morphological rearrangement while finding the new equilibrium configuration. This rapid cooling is known as a *quench* and the resultant change of the system from a one-phase to a two-phase morphology is called *coarsening*. Here we use Landau theory to analyze the non-equilibrium dynamics which take place during this transition.

We derive a dynamical equation describing the time evolution of the field  $\phi(\mathbf{x})$  by combining the relations (2.3) and (2.4) with the equation for local material conservation.  $\phi$  is locally conserved, and thus obeys the continuity equation

$$\partial_t \phi + \nabla \cdot \mathbf{j}_\phi = 0, \quad (2.14)$$

which results in what is known as the *generalized diffusion equation*

$$\partial_t \phi = m \nabla^2 \frac{\delta F}{\delta \phi}. \quad (2.15)$$

Taking for  $F$  a general form of the Landau free energy results in

$$\partial_t \phi = m \nabla^2 \left( \frac{\partial f}{\partial \phi} - \kappa \nabla^2 \phi \right). \quad (2.16)$$

Because the free energy density  $f(\phi, T)$  is in general nonlinear this equation is often analytically intractable. However, we can get some information about the short-term dynamics of a system near a *fixed point* through the technique of *linear stability analysis*. Fixed points are states of the system that do not change with time, i.e. when  $\partial_t \phi = 0$ . Using stability analysis we can determine how the system will respond to infinitesimal perturbations, which are always present in a real system at non-zero temperature.

First, we see that the equation has a fixed point when  $\phi(\mathbf{x}, t) = \Phi_0$ , i.e. when the system is homogeneous or *well-mixed*. Linearizing about this point we set  $\phi(\mathbf{x}, t) = \Phi_0 + \epsilon(\mathbf{x}, t)$ , where  $\epsilon$  is a field of infinitesimal perturbations. This results in

$$\partial_t \epsilon = m \nabla^2 (b_2 - \kappa \nabla^2) \epsilon, \quad (2.17)$$

where

$$b_2 = \left. \frac{\partial^2 f}{\partial \phi^2} \right|_{\Phi_0}. \quad (2.18)$$

The linearized partial differential equation is converted into an eigenvalue equation

$$\partial_t \tilde{\epsilon} = \lambda(q) \tilde{\epsilon} \quad (2.19)$$

by taking the Fourier transform of the spatial variables  $\tilde{\epsilon}(\mathbf{q}) = \mathcal{F}\epsilon(\mathbf{x})$ , with

$$\lambda(q) = -m\mathbf{q}^2 (b_2 + \kappa\mathbf{q}^2) . \quad (2.20)$$

Then making the transformation to dimensionless variables  $q \rightarrow q/L$  and  $\lambda \rightarrow \lambda/T$  we can form the dimensionless groups  $mT|b_2|/L^2$  and  $\kappa/|b_2|L^2$ . From these we derive a characteristic length  $L = \sqrt{\kappa/|b_2|}$  and characteristic time  $T = \kappa/m|b_2|^2$ . We now write eq. (2.20) in dimensionless form as

$$\lambda(q) = -\mathbf{q}^2 (\pm 1 + \mathbf{q}^2) , \quad (2.21)$$

which we plot in fig. 2.4.

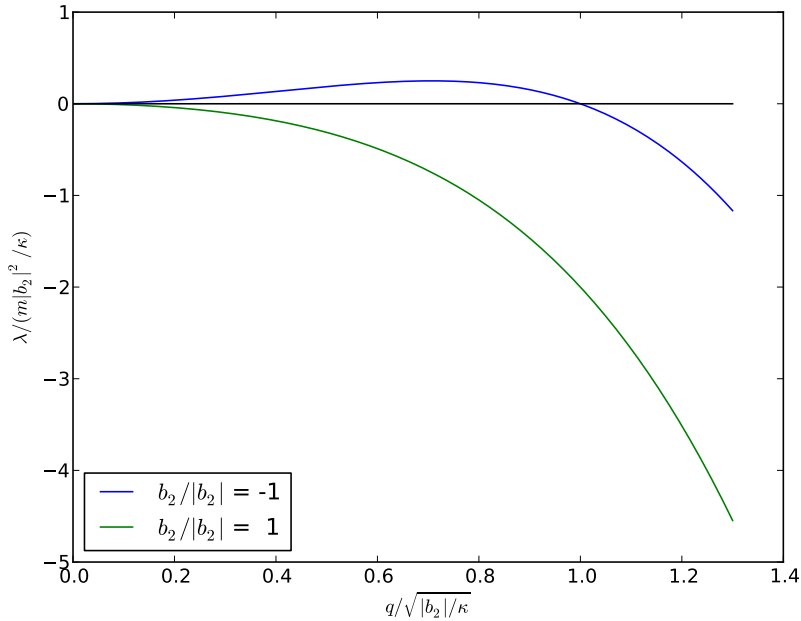


Figure 2.4: Growth rate  $\lambda$  of sinusoidal perturbation as a function of wavenumber. Linear stability analysis gives the growth rate as  $\lambda(q) = -\mathbf{q}^2 (\pm 1 + \mathbf{q}^2)$ . When  $b_2 < 0$  positive growth rates exists for some frequencies (see blue line) and the homogeneous state  $\phi(x) = \Phi_0$  is unstable, leading to coarsening and phase separation.

Modes  $q$  which result in  $\lambda > 0$  are unstable and will grow initially, while modes that give  $\lambda < 0$  are stable and will not grow. The existence of unstable

modes implies that a simple one-phase equilibrium solution is not possible and the system will phase separate. From this we can see that the condition  $b_2 < 0$  is necessary – although not sufficient – for the homogeneous state to be stable.

Regions of  $f(\phi)$  with negative curvature are linearly unstable to infinitesimal perturbations and homogeneous systems with  $\Phi_0$  in this region proceed spontaneously to separate into two phases. This spontaneous demixing process is called *spinodal decomposition*. There is another coarsening process distinct from spinodal decomposition that is not amenable to linear stability analysis. When a system is stable with respect to infinitesimal perturbations, but is not in equilibrium we say that it is *metastable*. This leads to a different kind of coarsening dynamics called *nucleation and growth* where large fluctuations are necessary in order to begin the transition to equilibrium.

In the quartic model free energy density the instability condition  $b_2 < 0$  can be rewritten as

$$T < T_c - 6b\phi^2. \quad (2.22)$$

We show this region in the phase plot in figure 2.2 highlighted in red. The line defined by  $b_2 = 0$  – the inflection points of  $f$  – is called the *spinodal*. The area between the spinodal and binodal is the region of metastability, where quenched systems coarsen via nucleation and growth. Below the spinodal is the purely unstable region, where quenched systems coarsen via spinodal decomposition.

In real systems the large fluctuations necessary to bring a metastable system to equilibrium arise naturally from the randomness inherent in thermal systems. In the next chapter we develop a simple, stochastic molecular model capable of exploring both of these coarsening processes.

## 2.4 Chemical reactions

One aim of this thesis is to explore how chemical reactions affect these coarsening processes. In this section we introduce a simple extension of the model to accounting for chemical turnover.

An additional term  $R(\phi)$  describing this turnover is added to the dynamical equation (2.16) giving

$$\partial_t \phi = m \nabla^2 \frac{\delta F}{\delta \phi} + R(\phi). \quad (2.23)$$

The functional form of  $R(\phi)$  depends on the type of chemical kinetics at play, but in general the rates are derived from the stoichiometric description via the law of mass action. For example, the first order reactions  $A \xrightleftharpoons[k_{BA}]{k_{AB}} B$  are described by the rate equations

$$\begin{aligned} \partial_t \phi_A &= -k_{AB}\phi_A + k_{BA}\phi_B \\ \partial_t \phi_B &= -k_{BA}\phi_B + k_{AB}\phi_A, \end{aligned}$$

which can be rewritten in terms of  $\phi$  as

$$R = \partial_t \phi_A - \partial_t \phi_B = k_{BA} - k_{AB} - (k_{BA} + k_{AB})\phi. \quad (2.24)$$

First-order reactions result in a rate function  $R(\phi)$  that is first-order in  $\phi$ . Likewise second-order reactions result in a second-order rate function. Here we replace  $R(\phi)$  in (2.23) with the more explicit form in terms of the first order rate constants

$$\partial_t \phi = m \nabla^2 \frac{\delta F}{\delta \phi} - (k_{BA} + k_{AB})\phi + (k_{BA} - k_{AB}), \quad (2.25)$$

Later in this thesis we will investigate the effects of both first and second-order reactions on the dynamical and steady-state behavior of active, one and two-phase systems.

It should be made clear that the method used here to account for chemical reactions is valid only in a description of *active systems*. That is the energy required to drive the chemical reactions can be seen as coming either from inside the system (ex. via the consumption of a molecular fuel like adenosine triphosphate) or outside the system as in the case of a light source powering photo-activated reactions.

Because we are dealing with active systems an important distinction must be made between true thermodynamic equilibrium, in which there are no net fluxes of material or energy, and the less restrictive case of steady-state behavior, in which fluxes may exist but are constant in time. In our discussion of chemically active systems we restrict ourselves to the latter.

# Chapter 3

## Lattice model

In this chapter we develop a simple, stochastic molecular model which will allow us to explore the dynamics of an active, phase-separating fluid with chemical reactions and thermal fluctuations.

The discrete nature of the model allows for a simple account of the local attractive and chemical interactions, as well as for simple algorithms to simulate the stochastic, diffusive motion.

### 3.1 Definition of lattice model

We begin with a square 2D lattice  $\mathbf{g} = \{g_1, g_2, \dots, g_N\}$  with a particle at every vertex  $v$  taking on one of two types  $g_v \in \{A, B\}$ . An energy  $J_{g_v g_{v'}}$  is associated with each pair of nearest neighbors  $\langle v, v' \rangle$  which results in a total configurational energy

$$\mathcal{H}(\mathbf{g}) = \sum_{\langle v, v' \rangle} J_{g_v g_{v'}} \quad (3.1)$$

The sum is over all pairs of nearest neighbors on a square lattice with periodic boundaries, such that every vertex has degree four. We define the energy  $J_{g_v g_{v'}}$  associated with each pair to have  $A \leftrightarrow B$  symmetry

$$J_{AB} = J_{BA} \quad (3.2)$$

$$J_{AA} = J_{BB} \quad (3.3)$$

We are interested in non-equilibrium dynamics of coarsening processes and the dependence of these properties on environmental parameters like temperature, local energetic interactions  $J_{g_v, g_{v'}}$  and chemical reaction rates. When switching from a continuous description in terms of a continuous order parameter  $\phi$  to a fully discrete system we need a new method for mathematically describing the system's phase properties. In the continuous model systems with

phase coexistence are characterized by an order parameter which is not constant in space. In the lattice model the variables which define a configuration of the grid take on discrete values (A or B), so the conditions describing phase coexistence must be stated in terms of some spatially averaged quantity. Also, systems described by the same set of macroscopic parameters have different instantaneous morphologies, which requires that we look at quantities which average over an ensemble of states.

There are many different quantities one may use to characterize the coarsening process in such models which take these considerations into account. The configurational energy, droplet size distribution, two-point correlation function and structure factor are all capable of extracting similar information [1]. We will predominantly use the structure factor  $S$  defined

$$S(\mathbf{q}) = \frac{1}{N_A} \left\langle \sum_{m,n} \exp(i\mathbf{q}(\mathbf{R}_m - \mathbf{R}_n)) \right\rangle, \quad (3.4)$$

where  $N_A$  is the number of A particles and both  $m$  and  $n$  are indices which run over each A particle in the system. The variable  $\mathbf{R}_m$  is the position vector for the  $m$ th A particle with units of length and  $\mathbf{q}$  is the Fourier pair or  $\mathbf{R}$ . The angle brackets above represent an average over an ensemble of systems. For fluid systems isotropic symmetry allows us to reduce  $S$  to a function of scalar  $q$ . The structure factor gives the distribution of Fourier modes in the system, and thus is a measure of the typical size of regions or *domains* of a certain phase. As the system changes over time these domains will move and change in size, and this will be reflected by changes in the structure factor.

## 3.2 Equilibrium properties

### 3.2.1 Equilibrium statistical mechanics

As we transition from a coarse grained, continuous description of the system to one in terms of microscopic variables we must also switch from a purely thermodynamical description to a statistical mechanical description. In this section we develop that description and relate it to the continuum model when possible. This will enable us to more easily compare the predicted behavior resulting from these different classes of models.

The free energy of a system is given according to statistical mechanics as

$$F = -k_B T \ln Z, \quad (3.5)$$

where  $Z$  is the partition function. For the lattice model it takes the form

$$Z = \sum_{\text{states}} e^{-\beta \mathcal{H}(\mathbf{g})}, \quad (3.6)$$

where the sum is taken over all lattice configurations subject to the constraint that the total number of A and B particles is conserved. This free energy is

minimized at equilibrium, where the probability of observing any state of the grid  $\mathbf{g}$  is then given by the Boltzmann distribution

$$P(\mathbf{g}) = \frac{1}{Z} e^{-\beta \mathcal{H}(\mathbf{g})}, \quad (3.7)$$

which is the energy distribution which maximizes entropy. We will be interested in other thermodynamic quantities in addition to the free energy. The value at equilibrium of some quantity  $f(\mathbf{g})$  of the system is given by its expected value under the Boltzmann probability distribution

$$\langle f \rangle = \frac{1}{Z} \sum_{states} f(\mathbf{g}) e^{-\beta \mathcal{H}(\mathbf{g})}. \quad (3.8)$$

Calculating  $\langle f \rangle$  is difficult to perform analytically because of its enormous complexity. The length of the sum in the partition function is equal to the number of possible permutations of the grid, which scales as  $n^2!$ ,  $n$  being the number of vertices or (equivalently) the number particles on a side of the grid. The difficulty in calculations of this type necessitates the use of computer simulations.

### 3.2.2 Metropolis algorithm for computing ensemble averages

One of the principle methods of numerically attacking a calculation of the form (3.8) is via *Markov Chain Monte Carlo* integration [3]. These are a class of techniques in which a random sequence of states  $(\mathbf{g}^{(1)}, \mathbf{g}^{(2)}, \dots, \mathbf{g}^{(n)})$  of the lattice is generated, and the quantity of interest  $\langle f \rangle$  is obtained as a direct average over the  $N$  states in this sequence, i.e.

$$\langle f \rangle \approx \frac{1}{N} \sum_i^N f(\mathbf{g}^{(i)}), \quad (3.9)$$

where the approximation becomes exact in the limit  $N \rightarrow \infty$  assuming that the number of times a state appears in the chain is proportional to its true probability in the distribution  $P(\mathbf{g})$  we wish to sample. This is achieved by ensuring that the transition probabilities  $\omega(\mathbf{g} \rightarrow \mathbf{g}')$  satisfy a condition called *detailed balance*

$$\frac{P(\mathbf{g})}{P(\mathbf{g}')} = \frac{\omega(\mathbf{g}' \rightarrow \mathbf{g})}{\omega(\mathbf{g} \rightarrow \mathbf{g}')}. \quad (3.10)$$

Under the Boltzmann distribution this ratio of probabilities is equal to

$$\frac{P(\mathbf{g})}{P(\mathbf{g}')} = e^{-\beta \Delta \mathcal{H}}, \quad (3.11)$$

where  $\Delta \mathcal{H} = \mathcal{H}(\mathbf{g}') - \mathcal{H}(\mathbf{g})$ . While an infinite number of possible values for the individual transition probabilities will satisfy this ratio, the maximum probability one can choose is

$$\omega(\mathbf{g} \rightarrow \mathbf{g}') = \min(e^{-\beta \Delta \mathcal{H}}, 1) , \quad (3.12)$$

often called the *Metropolis probability*. If the current state of a Markov chain is  $\mathbf{g}^{(i)}$  we choose the next element in the following way. First a comparison state  $\mathbf{g}'$  is chosen at random – exactly how the comparison state is chosen we will cover in the next section. We set the next state in the chain  $\mathbf{g}^{(i+1)}$  according to the following rule

$$\mathbf{g}^{(i+1)} = \begin{cases} \mathbf{g}' & \text{if } \text{rand}(0, 1) < \omega(\mathbf{g}^{(i)} \rightarrow \mathbf{g}') \\ \mathbf{g}^{(i)} & \text{if } \text{rand}(0, 1) \geq \omega(\mathbf{g}^{(i)} \rightarrow \mathbf{g}') \end{cases} \quad (3.13)$$

where the number  $\text{rand}(0, 1)$  is a random number evenly distributed on the interval  $[0, 1]$ . This is a very simple procedure for a computer to perform which allows us to quickly sample a large number of states. The necessary number of states of course depends on the nature of the probability distribution we want to replicate, the properties of the quantity  $\langle f \rangle$  in which we are interested, and the desired accuracy. Note that this technique is intended to sample equilibrium properties of the system. In our study of phase transitions we are also interested in dynamic properties. In section (3.3) we shall see how to extend this technique in order to obtain information about dynamical quantities.

### 3.2.3 Relationship to continuous description

The mean-field free energy for such a model depends solely on the fraction  $\phi_A = N_A/n^2, \phi_B = N_B/n^2$  of A and B particles present in the lattice. The expected energy per nearest neighbor pair is then

$$u = J_{AA}\phi_A^2 + J_{BB}\phi_B^2 + 2J_{AB}\phi_A\phi_B . \quad (3.14)$$

The entropic component of the free energy is given by the *entropy of mixing*, which results in an entropy per vertex

$$s = -k_B \sum_{i \in \{A, B\}} p_i \ln p_i = -k_B (\phi_A \ln \phi_A + \phi_B \ln \phi_B) . \quad (3.15)$$

Taking the thermodynamic limit results in a free energy density

$$f(\phi_A, \phi_B) = J_{AA}\phi_A^2 + J_{BB}\phi_B^2 + 2J_{AB}\phi_A\phi_B + k_B T \frac{1}{2} k_B (\phi_A \ln \phi_A + \phi_B \ln \phi_B) . \quad (3.16)$$

Using the linear relations

$$\phi_A = \frac{1}{2} (1 + \phi) \quad (3.17)$$

$$\phi_B = \frac{1}{2} (1 - \phi) \quad (3.18)$$

we can write  $f$  as a function solely of  $\phi$

$$f(\phi) = -\frac{1}{4}\Omega\phi^2 + \frac{1}{4}k_B T ((\phi + 1)\log(\phi + 1) + (1 - \phi)\log(1 - \phi)) , \quad (3.19)$$

where we have removed additive constants and defined

$$\Omega \equiv (2J_{AB} - J_{AA} - J_{BB}) \quad (3.20)$$

Here  $\Omega$  can be thought of as the energy change per vertex when an A-A pair and an B-B pair are converted into two A-B pairs. If  $\Omega$  is positive then segregation of components is energetically beneficial, and can dominate the behavior at low temperature where entropic effects are negligible. If  $\Omega$  is negative then the components want to mix, and the system will be homogeneous for all temperatures. The free energy (3.19) is symmetric in  $\phi$ . This potential also exhibits a transition from a single well to a double well shape as we lower the temperature beyond its critical value (figure 3.1), which we determine by the condition that the second derivative of  $f$

$$\partial_\phi^2 f(\phi, T) = \frac{1}{2}\Omega + \frac{1}{4}k_B T \left( \frac{2}{1 - \phi^2} \right) \quad (3.21)$$

is zero at  $\phi = 0$ , which leaves

$$k_B T_c = \Omega . \quad (3.22)$$

In figure 3.1 we plot the free energy density derived from this lattice model for various values of the temperature near  $T_c$ . The conditions determining the binodal and spinodal lines are the same as (2.11) for the simple quartic free energy density (2.9)

$$-\phi_m < \Phi_0 < \phi_m \quad (3.23)$$

where  $\pm\phi_m$  are the potential minima. In this case we cannot solve for the function  $\phi_m(T, \Omega)$  explicitly, however we can still create the phase plot using

$$k_B T_m(\phi, \Omega) = \frac{2\phi\Omega}{\log(\phi + 1) - \log(1 - \phi)} \quad (3.24)$$

where  $T_m$  is the temperature along the binodal line. From the above free energy  $f(\phi)$  we derive the following phase diagram (figure 3.2), showing the one and two phase regimes as a function of temperature and average volume fraction  $\Phi_0$ . We have also highlighted within the two-phase region the areas corresponding to the different coarsening processes.

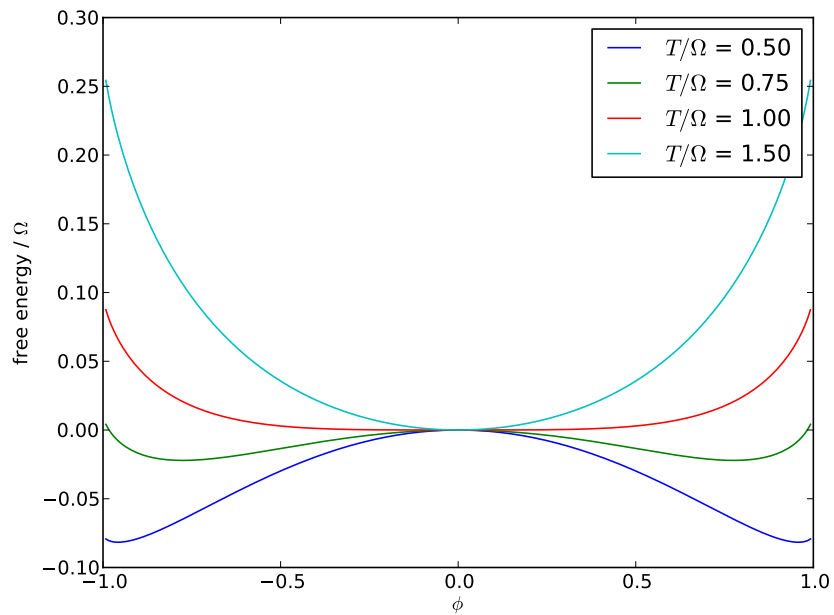


Figure 3.1: free energy density as a function of composition  $\phi$  derived from the mean-field, continuum limit of the lattice model for various values of the temperature near  $T_c = \Omega$ .

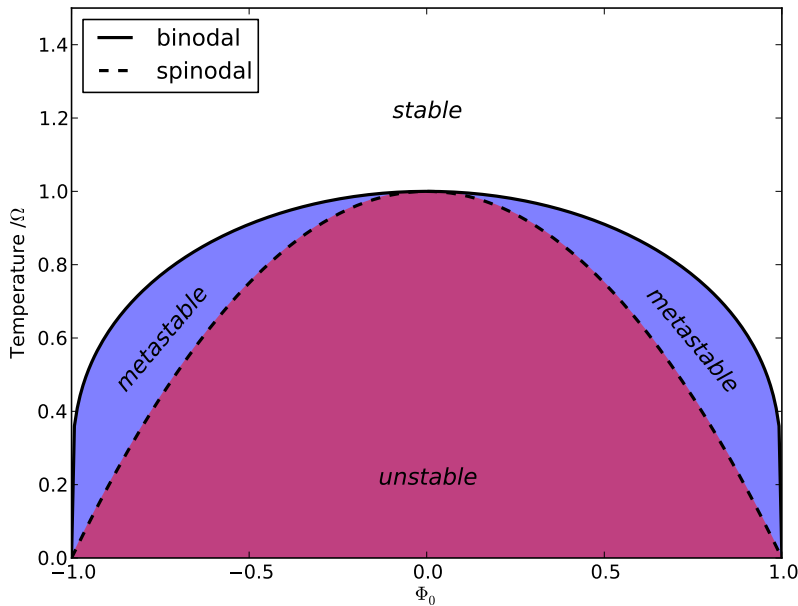


Figure 3.2: Phase portrait showing stable, unstable and metastable regions of phase space as a function of temperature and composition  $\Phi_0$ . The binodal and spinodal lines are taken from the free energy density (3.19) which we have derived from the lattice model under the mean-field approximation in the continuous limit. The phase portrait is qualitatively similar to that from the simple, quartic free energy density used in chapter 2 (see figure 2.2). Above the binodal the equilibrium state has single, homogeneous phase. Beneath it the equilibrium state has coexisting phases. Beneath the spinodal a homogeneously prepared system is unstable and coarseens via spinodal decomposition. Between the spinodal and binodal a homogeneously prepared system is metastable and coarseens via nucleation and growth.

### 3.3 Nonequilibrium dynamics via Kawasaki exchange

We also investigate the dynamics of phase separation in the absence of advective currents, when thermal forces drive the motion of the particles. We consider initially homogeneous systems which are not yet in equilibrium. In order to simulate the system's progression towards equilibrium as a Markov process we associate each transition in the sequence  $(\mathbf{g}^{(1)}, \mathbf{g}^{(2)}, \dots, \mathbf{g}^{(n)})$  with a length of time  $\tau$ . In order to interpret the sequence of states as the time evolution of the system towards equilibrium the transition probabilities  $\omega$  must satisfy two conditions.

1. The detailed balance condition (3.10). This ensures that the equilibrium state is stable.
2. The probability distribution  $p_v$  for a particle on the grid satisfies the diffusion equation in some appropriate limit.

the difference in the probability that the particle  $v$  can be found at  $\mathbf{r}$  evolves according to

$$\begin{aligned} p_v(\mathbf{r}, t + \tau) - p_v(\mathbf{r}, t) &= \frac{-2}{n^2} p_v(\mathbf{r}, t) + \frac{1}{2n^2} [p_v(\mathbf{r} + \Delta\mathbf{x}_1, t) + p_v(\mathbf{r} - \Delta\mathbf{x}_1, t) \\ &\quad + p_v(\mathbf{r} + \Delta\mathbf{x}_2, t) + p_v(\mathbf{r} - \Delta\mathbf{x}_2, t)] , \end{aligned} \quad (3.25)$$

where the first term on the right hand side represents the flux of probability away from the point  $\mathbf{r}$ , and the second term in parenthesis represents the flux from the neighboring vertices in to the point  $\mathbf{r}$ . The perpendicular displacement vectors  $\Delta\mathbf{x}_1$  and  $\Delta\mathbf{x}_2$  have length  $\ell$ . We can rewrite the right hand side as the sum of two terms, each of which is a discrete second derivative

$$\begin{aligned} \frac{p_v(\mathbf{r}, t + \tau) - p_v(\mathbf{r}, t)}{\tau} &= \frac{\ell^2}{\tau E} \left[ \frac{p_v(\mathbf{r} + \Delta\mathbf{x}_1, t) - 2p_v(\mathbf{r}, t) + p_v(\mathbf{r} - \Delta\mathbf{x}_1, t)}{\ell^2} \right. \\ &\quad \left. + \frac{p_v(\mathbf{r} + \Delta\mathbf{x}_2, t) - 2p_v(\mathbf{r}, t) + p_v(\mathbf{r} - \Delta\mathbf{x}_2, t)}{\ell^2} \right] , \end{aligned} \quad (3.26)$$

then taking the limits  $\ell \rightarrow 0$  and  $\tau \rightarrow 0$  we arrive at the diffusion equation

$$\partial_t p_v = D \nabla^2 p_v . \quad (3.27)$$

Here we have replaced  $\ell$  and  $\tau$  using the equality

$$D = \frac{\ell^2}{2n^2\tau} . \quad (3.28)$$

The key point in our derivation of (3.27) was that particles explore the lattice via the random exchange of nearest neighbors, a process called *Kawasaki exchange* [17]. This process is an undirected random walk, well known to result in diffusive motion. We should note that purely diffusive motion is only the behavior we expect from the system when the inter-particle energetic interactions are weak, resulting in currents which are driven by entropic effects. This is taken into account in the derivation above by assuming that the probability of flipping nearest neighbors is independent of the type of particles flipped.

Now,  $l$  and  $n$  is the number of vertices on a side. We write the probability distribution of a single particle  $v$  at position  $\mathbf{r}$  on the lattice at a time  $t$  as  $p_v(\mathbf{r}, t)$ . If we select a pair of nearest neighbors at random from the grid and flip them then

## 3.4 Chemical reactions on the lattice

In this section we cover the procedure of adding chemical reactions to the lattice simulation. This boils down to assigning the probabilities  $P(A \rightarrow B, \tau)$  and  $P(B \rightarrow A, \tau)$  that a particle will switch type within the span of one timestep  $\tau$  as a function of its local, microscopic environment.

### 3.4.1 First order reactions

For the case of first order reactions  $A \xrightleftharpoons[k_{BA}]{k_{AB}} B$  the particles undergo reactions without the aid of a catalyst. In the lattice model this means that the probabilities  $P(A \rightarrow B, \tau)$  and  $P(B \rightarrow A, \tau)$  are independent of the types of neighbors the particle has on the grid. Also for first order reactions a direct correspondence can be drawn between this probability and the macroscopic reaction rates  $k_{AB}$  and  $k_{BA}$  by solving equation (2.25) in the mean field approximation.

$$\phi(t) = \frac{\Gamma_2}{\Gamma_1} + \left( \phi_0 - \frac{\Gamma_2}{\Gamma_1} \right) e^{-\Gamma_1 t} \quad (3.29)$$

where  $\Gamma_1 = k_{BA} + k_{AB}$  and  $\Gamma_2 = k_{BA} - k_{AB}$  and  $\phi_0 = \phi(t=0)$ . We transform this equation using the linear relations (3.17). Under the mean field approximation the probability of finding a particle of type A (B) at any point on the lattice is equal to  $\phi_A$  ( $\phi_B$ ). Using the initial conditions for A particles  $\phi_0 = 1$  and for B particles  $\phi_0 = -1$  then leaves us with the following probabilities

$$P(A \rightarrow B, t) = \frac{1}{2} \left( 1 - \frac{\Gamma_2}{\Gamma_1} \right) (1 + e^{-\Gamma_1 t}) \quad (3.30)$$

$$P(B \rightarrow A, t) = \frac{1}{2} \left( 1 + \frac{\Gamma_2}{\Gamma_1} \right) (1 - e^{-\Gamma_1 t}) \quad (3.31)$$

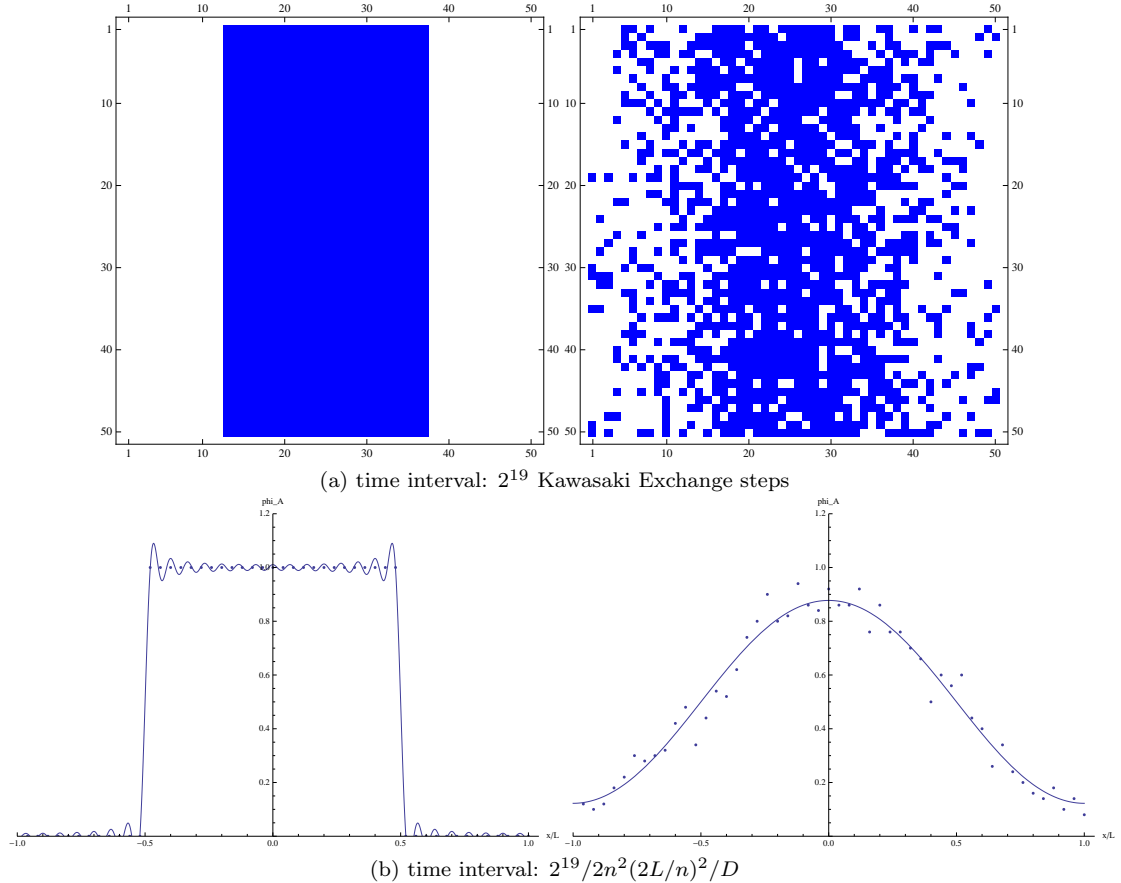
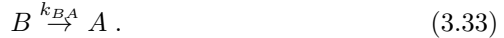


Figure 3.3: (a) Diffusive dynamics via Kawasaki exchange algorithm from square initial conditions with side length of  $n = 50$  grid points. (b) The average of the grid along vertical dimension is compared with the analytic solution to the diffusion equation over a space of length  $2L$ , the time intervals above agree in accordance with equation (3.28).

### 3.4.2 Autocatalytic reactions

We also investigate the non-symmetric case of *autocatalytic* second order reactions



The evolution of the field  $\phi(x)$  is then described by

$$\partial_t \phi = m \nabla^2 \frac{\delta F}{\delta \phi} + k_q \phi^2 - k_{BA} \phi - k_q + 1 \quad (3.34)$$

When the field can be approximated as homogeneous  $\phi(x) = \Phi$  the equations describing the growth of the average composition  $\Phi$  reduce to

$$\partial_t \Phi = k_q \Phi^2 - k_{BA} \Phi - k_q + k_{BA} . \quad (3.35)$$

This equation is nonlinear and a solution  $\Phi(k_q, k_{BA}, t)$  only exists in the limit when the timescale for reactions is much longer than that for diffusion, such that  $k_q \tau \ll 1$ . Equating the rates above with that given from the lattice model under the mean-field approximation we find that

$$P(A \rightarrow B) = \frac{1}{4} k_q C_B(v) t \quad (3.36)$$

$$P(B \rightarrow A) = k_{BA} t , \quad (3.37)$$

where  $C_B$  is the number of B neighbors the particle has. This agrees with our understanding of the molecular process in that if an A particle has more B neighbors it is increasingly likely to react with one of them.



## Chapter 4

# Stationary state morphology

In this chapter we investigate the steady state properties of the lattice model. We are interested in the dependence of a system's morphology on its temperature, composition and reaction rates. By performing Monte Carlo simulations of the lattice model we will be able to visualize this morphology and quantify important properties like the structure factor  $S(q)$  and average composition  $\Phi$ . All simulations are performed using the Kawasaki exchange method for simulating the diffusive dynamics, while the chemical reaction dynamics are performed using the methods described in the previous chapter, (see eqs. (3.37 and 3.31)). For our purposes a system is defined to be in stationary state when the mean wavenumber  $\langle q \rangle$  and the average composition  $\Phi$  are constant in time. Limited computational power prevents restricts the length of time which we are capable of simulating for systems of a given size, which limits our ability to a steady state. Additionally, our ability to judge whether a system has reached steady state is complicated by the fluctuations which are inherent in the Metropolis algorithm (3.12).

### 4.1 Passive system

The sequence in figure 4.1 shows the evolution of two phase-separating systems through time, along with their structure factors. We see how the systems coarsen with time and how the structure factor is a capable measure of this coarsening. The systems differ in their temperature, and we clearly see that increasing the temperature tends to blur the boundaries between phases as interfacial energy minimization becomes less important to the total free energy. This is also reflected in the structure factor, where a single well defined peak only exists at lower temperatures.

According to mean-field theory the equilibrium morphology of the passive lattice model is a function of scaled temperature  $T/\Omega$  and composition  $\Phi_0$  (see

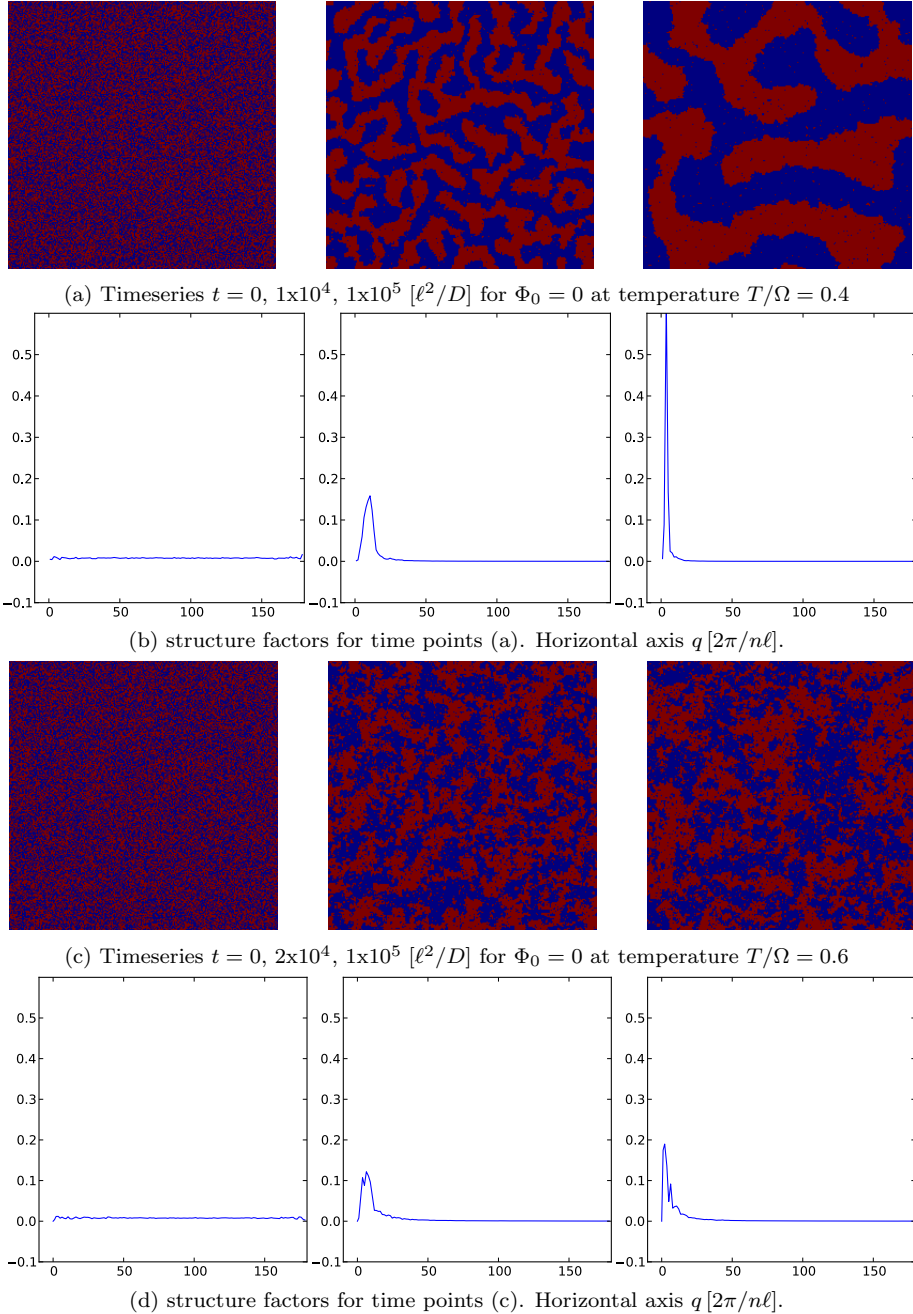


Figure 4.1: Red (Blue) = A (B) type particles. Blue curves show structure factor defined (3.4). Panels (a) & (b) for system with scaled temperature  $T/\Omega = 0.4$ . Panels (c) & (d) for system with scaled temperature  $T/\Omega = 0.6$ . Square grids with side length  $n = 256$ .

fig 3.2). Systems with temperature above  $k_B T_c = \Omega$  are homogeneous (see eq. (3.22)). Then, as the temperature is lowered the system is expected to undergo a continuous transition into the two phase region and phases of differing composition coexist in equilibrium. We ran simulations of the lattice model over a range of temperatures and compositions, exploring the equilibrium morphology and making comparisons to mean field theory. In figure 4.2 we show systems near equilibrium for differing values of  $T$  and  $\Phi$ .

At low temperature we also expect the equilibrium morphology to be governed by the minimization of interfacial energy, and less by entropic effects. In the limit where the minimization of surface energies dominates completely we expect “soap bubble” morphologies, where the exact shape is governed by boundary conditions and the composition of system. We see in figure 4.2 that the interfaces dividing phases are sharper and more rounded at lower temperature (two systems on the right). For scaled temperature  $T/\Omega >> 1$  we expect a homogeneous morphology (see eq. 3.22). Again in figure 4.2 we see that the phase regions are gone for the higher temperature systems (on the left), and the system is homogeneous.

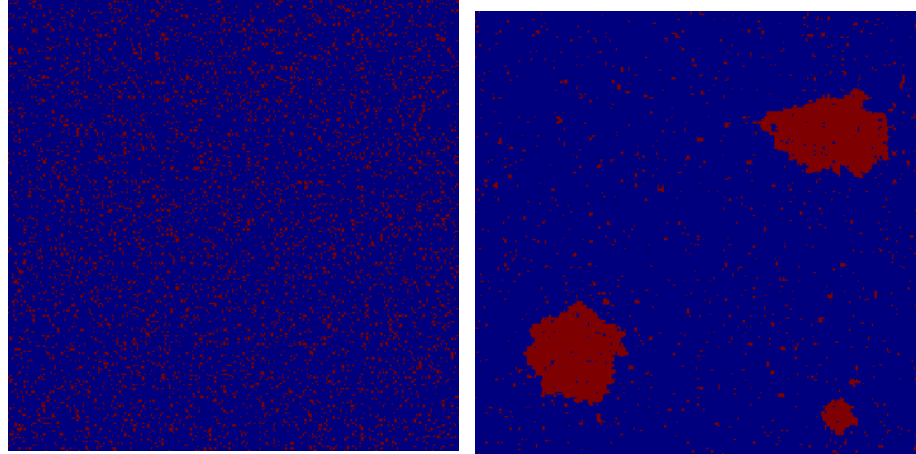
In figure 4.3 the mean value of the wavenumber  $\langle q \rangle$  is taken from the structure factor distribution and shown as a function of the scaled temperature  $T/\Omega$  and average volume fraction  $\Phi_0$ . We can see that  $\langle q \rangle$  undergoes a continuous transition over a range of temperatures centered about the critical temperature predicted from mean-field theory,  $T_c/\Omega = 1$ .  $\langle q \rangle$  is a measure of the (inverse) characteristic length of structures in the system. Smaller values indicate larger domains. In these grids with  $n = 256$  there is a maximum value ( $\approx 90$ ) which indicates that domains have a characteristic length which is the size of the lattice spacing i.e. that the system is completely mixed. The transition from the phase separated morphology to the homogeneous mixture takes place at lower temperatures for systems with greater  $|\Phi_0|$ . This is in agreement with the predictions of the mean field theory, and can be seen in the phase plot (figure 3.2) by following lines of decreasing temperature and constant  $\Phi_0$ . We also observe that the transition takes place *more rapidly* as the temperature is varied for systems with large  $|\Phi_0|$  while systems with  $\Phi \approx 0$  exhibit a longer, slower transition.

## 4.2 First Order Reactions

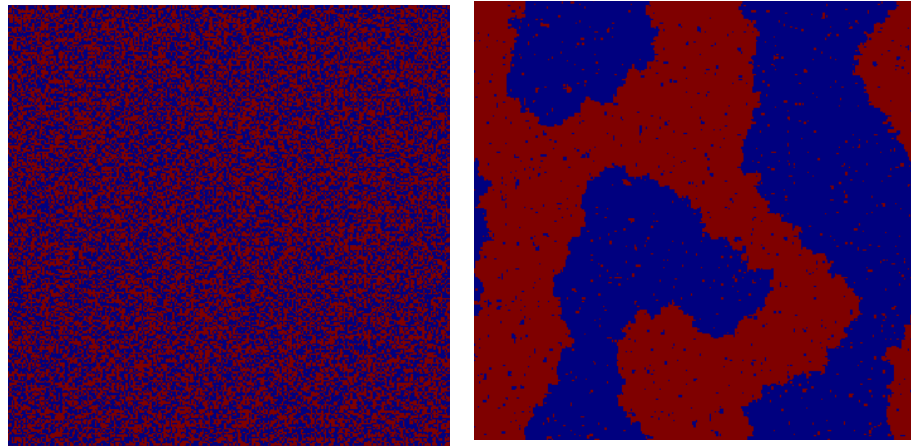
Here we investigate steady state morphologies of systems with first order  $A \leftrightarrow B$  reaction kinetics. In the continuous limit these steady states are solutions to eq. (2.23) with  $\partial_t = 0$ :

$$m\nabla^2 \frac{\delta F}{\delta \phi} - \Gamma_1 \phi + \Gamma_2 = 0 . \quad (4.1)$$

where  $\Gamma_1 = k_{AB} + k_{BA}$  is the symmetric rate and  $\Gamma_2 = k_{BA} - k_{AB}$  the asymmetric rate. These reaction rates completely determine the composition  $\Phi(t)$  through time and result in a steady state value



(a) Asymmetric composition  $\Phi_0 = -0.9$ . Temperature: Left  $T/\Omega = 1.5$ . Right  $T/\Omega = 0.4$



(b) Symmetric composition  $\Phi_0 = 0$ . Temperature: Left  $T/\Omega = 1.5$ . Right  $T/\Omega = 0.4$

Figure 4.2: Red (Blue) = A (B) type particles. Near equilibrium morphology,  $t = 5 \times 10^5 [\ell^2/D]$ . Square grids with side length  $n = 256$ . Other compositions and temperatures have been tested, but are not shown here.

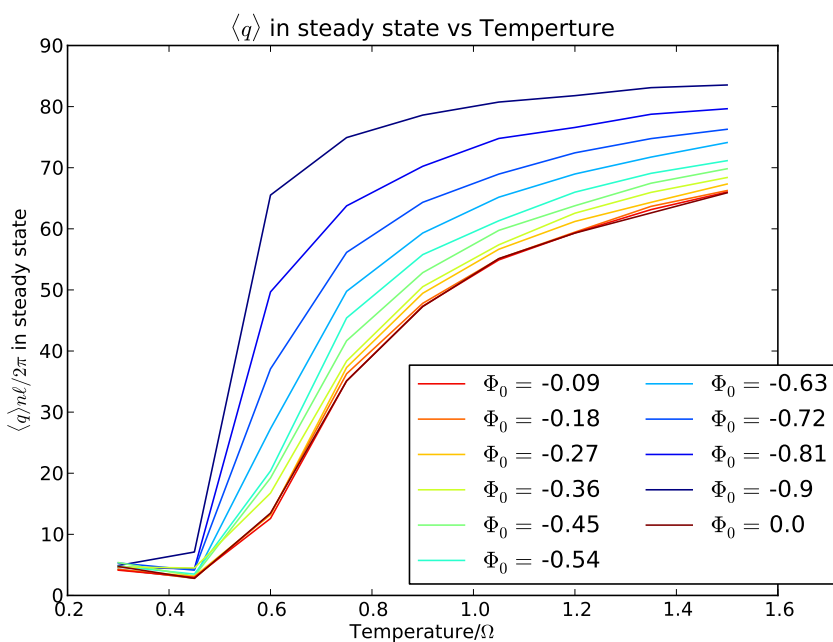


Figure 4.3: Mean wavenumber  $\langle q \rangle$  from the structure factor  $S(q)$  (3.4) as a function of temperature.  $\Phi_0$  is the composition, a constant in passive systems.

$$\Phi = \Gamma_2 / \Gamma_1 . \quad (4.2)$$

More interesting behavior is apparent in the affect of these reactions on spatial patterns in phase separating systems. It has been shown that the system is prevented from coarsening indefinitely when first-order reactions are introduced [10]. We can see this behavior clearly in figure 4.4, where we show systems of different  $\Gamma_1$  which have stopped coarsening. The asymmetric rate  $\Gamma_2$  is fixed at zero, which fixes the composition  $\Phi(t) = \Phi_0 = 0$ .

Systems with first order reactions maintain patterns of a characteristic size in steady state. In figure 4.4 we contrast systems with different symmetric, first-order reaction rates  $\Gamma_1$ . As  $\Gamma_1$  is increased the speed of mixing is increased relative to the speed of coarsening which causes the characteristic size of steady-state patterns to decrease.

In figure 4.5 we show the mean wavenumber  $\langle q \rangle$  in steady state which displays a clear dependence on  $\Gamma_1$ . Over a range of  $10^0 < \Gamma_1 \ell^2 / D < 10^4$  we see roughly logarithmic dependence of  $\langle q \rangle$  on  $\Gamma_1$ . There appears to be a critical rate above which the system is fully mixed and increasing the reaction rates further has no effect on the morphology. For small  $\Gamma_1$ ,  $\langle q \rangle$  is limited by the finite size of our simulation lattice and the finite simulation time, but we do not predict a fundamental theoretical limit to the maximum mean size of steady state patterns. The orange markers show the average volume fraction  $\Phi$ , which for the case of first order reactions agrees with the mean field result  $\Phi = \Gamma_2 / \Gamma_1$ . They are included here to contrast with the autocatalytic scenario.

### 4.3 Autocatalytic Reactions

Here we investigate steady state morphologies of systems with one autocatalytic and one first order chemical reaction



In the continuous limit these steady states are solutions to eq. (2.23) with  $\partial_t \phi = 0$

$$m \nabla^2 \frac{\delta F}{\delta \phi} + k_q \phi^2 - k_{BA} \phi - k_q + k_{BA} = 0 . \quad (4.5)$$

Considering a spatially constant field  $\phi(x)$  results in the steady state condition

$$k_q \phi^2 - k_{BA} \phi - k_q + k_{BA} = 0 . \quad (4.6)$$

We ran two sets of simulations for autocatalytic systems. In the first we vary the total rate  $k_{BA} + k_q$  while keeping the ratio  $k_q/k_{BA}$  fixed. In figure 4.6 we can see snapshots of the steady state behavior for three characteristic values

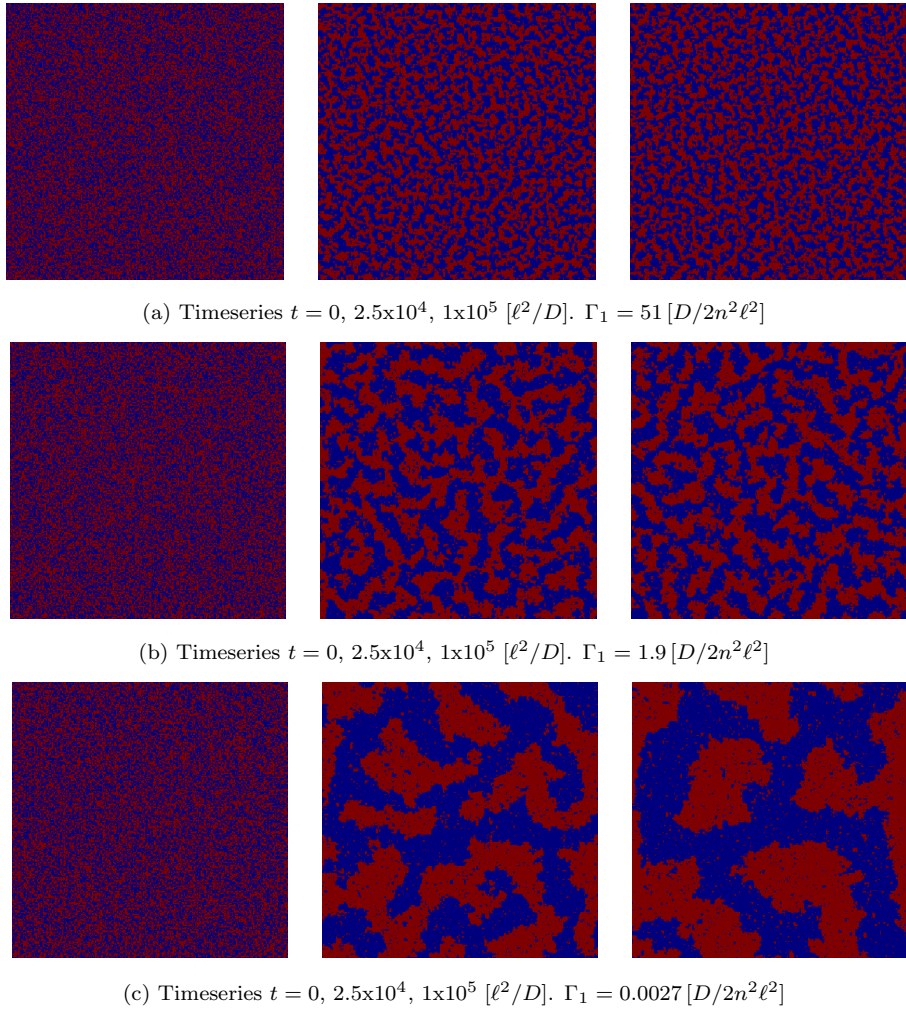


Figure 4.4: Red (Blue) = A (B) type particles. Average composition  $\Phi = 0$ . Temperature  $T/\Omega = 0.5$ . Three timeseries show systems with three different first-order reaction rates. Rates are listed under the panels and are higher for the upper panels.

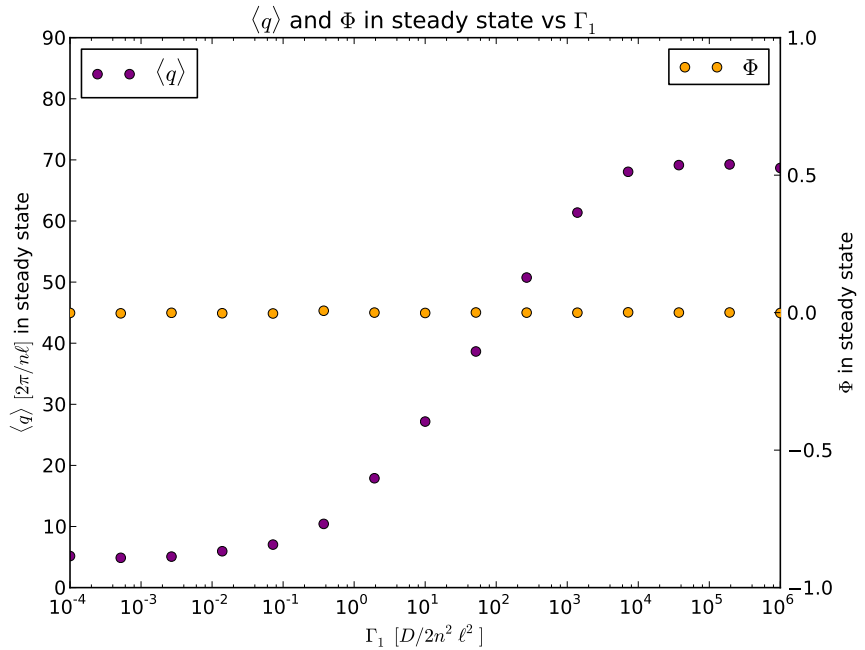


Figure 4.5: Left vertical axis (purple marks): mean wavenumber  $\langle q \rangle$  from structure factor (3.4) of autocatalytic system. Right vertical axis (orange marks): average composition  $\Phi$ . Horizontal axis: symmetric first-order reaction rate  $\Gamma_1 = k_{BA} + k_{AB}$ . Asymmetric rate fixed  $\Gamma_2 = k_{BA} - k_{AB} = 0$ . Temperature fixed  $T/\Omega = 0.5$

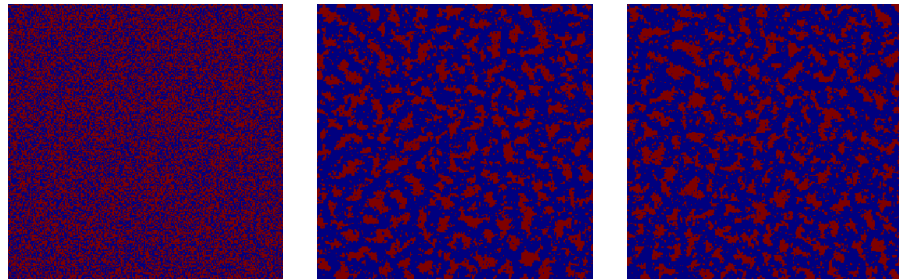
of the total rate. As in the case of first order reactions, the introduction of chemical turnover results in patterns of a finite mean wavelength to persist in steady state. Increasing the rate of this turnover relative to diffusion causes the characteristic scale of these patterns to decrease.

Additionally, in autocatalytic systems the average composition  $\Phi$  is related to the morphology. The autocatalytic reactions occur most frequently at the interface between phases, where the number of A-B edges is greatest. This allows the autocatalytic reactions to have a stronger effect in systems with smaller wavelength patterns as they also have more interfacial area. The net effect is that as the reaction rates are increased (while keeping the ratio  $k_q/k_{BA}$  constant) the fraction of B particles in the composition increases as can be seen in figure 4.6.

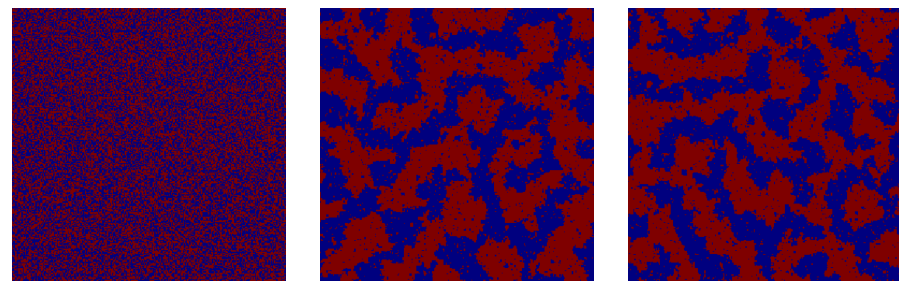
A quantitative comparison of the mean wavenumber from the structure factor  $\langle q \rangle$  and  $\Phi$  is made from these simulations and the results are shown in figure 4.7 as a function of  $k_{BA}$  for fixed ratio  $k_q/k_{BA} = 2$ .

As with first order reactions, the average mean wavenumber  $\langle q \rangle$  from the structure factor decreases as we increase the rate of reactions. Unlike in first-order systems we also see a clear, inverse relationship between  $\Phi$  in steady state and  $\langle q \rangle$ . We can understand this as an increase in the strength of the autocatalytic reactions when the system is well mixed, due to the increase in the number of A-B edges. Nonsmooth behavior of  $\langle q \rangle$  and  $\Phi$  in the range  $k_{BA}\ell^2/D < 0.01$  are transient artifacts, and are expected to disappear with longer simulations, when the system can get closer to steady state.

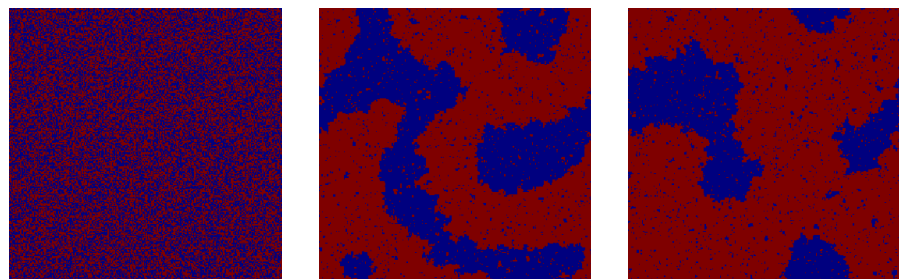
In the homogeneous field approximation we can make a prediction for  $\Phi$  in steady state which depends only on the ratio  $k_q/k_{BA}$ . The nonlinearities in (4.5) prevent a general analytical solution for  $\Phi(k_q, k_{BA})$  even in the limit  $t \rightarrow \infty$ . In figure 4.8 we explore the effect of the temperature on  $\Phi$  in steady for different values of  $k_q$ . The horizontal axis shows the ratio  $k_q/k_{BA}$ . We can see the role of the morphology clearly in this case, as the steady state  $\Phi$  varies over a wide range for systems with the same reaction rates, but different temperatures.



(a) Timeseries  $t = 0, 2.5 \times 10^4, 1 \times 10^5 [\ell^2/D]$ .  $k_q, k_{BA} = 200, 100 [D/2n^2\ell^2]$



(b) Timeseries  $t = 0, 2.5 \times 10^4, 1 \times 10^5 [\ell^2/D]$ .  $k_q, k_{BA} = 2.0, 1.0 [D/2n^2\ell^2]$



(c) Timeseries  $t = 0, 2.5 \times 10^4, 1 \times 10^5 [\ell^2/D]$ .  $k_q, k_{BA} = 0.02, 0.01 [D/2n^2\ell^2]$

Figure 4.6: Red (Blue) = A (B) type particles. Initial composition  $\Phi_0 = 0$ . Temperature  $T/\Omega = 0.5$ . Autocatalytic rate  $k_q$  and first order backrate  $k_{BA}$  vary between systems.

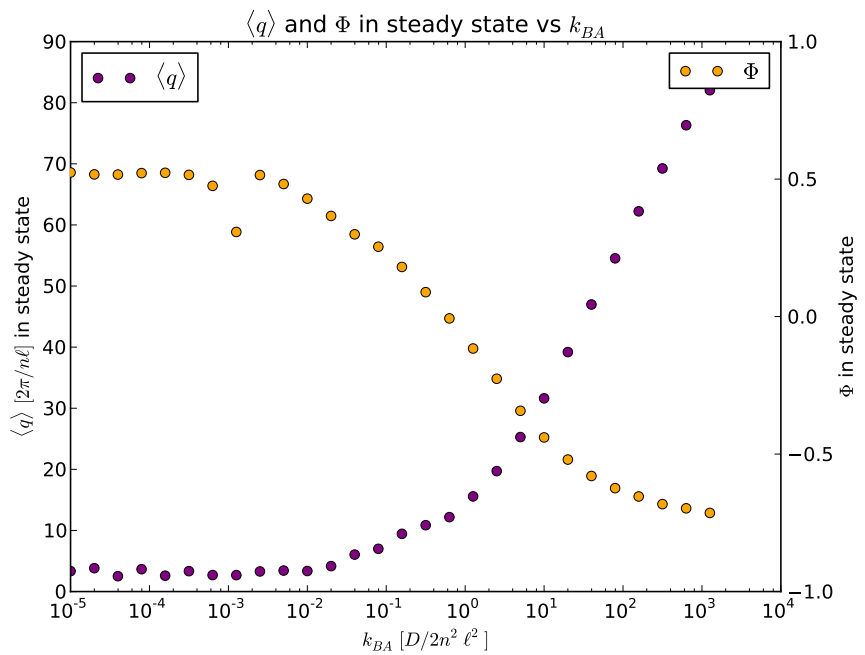


Figure 4.7: Left vertical axis (purple marks): mean wavenumber  $\langle q \rangle$  from structure factor (3.4) of autocatalytic system. Right vertical axis (orange marks): average composition  $\Phi$ . Horizontal axis:  $B \rightarrow A$  reaction rate  $k_{BA}$ , varied along line of constant  $k_q/k_{BA} = 2.0$ . Temperature is fixed at  $T/\Omega = 0.5$

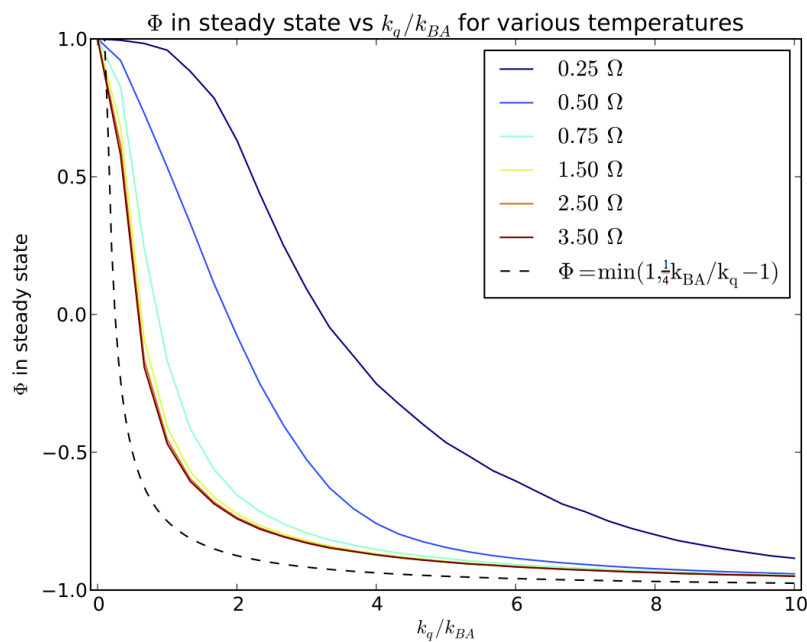


Figure 4.8: Average composition  $\Phi$  as a function of  $k_q$  (plotted as the ratio  $k_q/k_{BA} = 1 [D/2n^2\ell^2]$ ). Warmer colors show higher temperatures as given in the legend. Black dashed line gives mean-field prediction when  $\phi(\mathbf{x}) = \Phi$ .

## Chapter 5

# Coarsening Dynamics

In this chapter we investigate the dynamic properties of phase separating systems. We will focus on exploring the effects of chemical reactions on the coarsening process and on compositional changes to the system.

In the previous chapter we saw how chemical reactions could effectively halt the coarsening process at the cost of continued input of energy from an external source. However, we have not yet explored how the system approaches this steady state. Coarsening in both passive and active systems is driven by the systems desire to minimize the interfacial area between phases. However when chemical reactions are present the systems additionally undergo a mixing process which competes with coarsening. It can be helpful to view this competition as one between short-range attractive interactions and a *long-range repulsive interaction* between regions of similar phase [8] [10]. This will be helpful for our interpretation of the dynamics of chemically reactive systems in both the first-order and autocatalytic cases.

### 5.1 Passive systems

We know from Landau theory that coarsening continues indefinitely in passive systems, unless limited by system size (see section 2.2). We expect the structure factor to decrease in time, until it reaches a saturation point and halts. The average composition  $\Phi$  is an external parameter of the system in the absence of chemical reactions which allows us to study the behavior of  $\langle q \rangle$  alone. In this section we explore the dynamics of this coarsening, and investigate how this behavior depends on temperature and composition.

To investigate the effects of composition on these growth dynamics we ran simulations of the lattice model with temperature  $T/\Omega = 0.45$  for a range of compositions  $-0.9 < \Phi < 0$ . The morphology of two passive, phase-separating systems is shown in figure 5.1 over time for systems with compositions 0 and -0.9.

Although both systems are initially homogeneous, we see them undergo

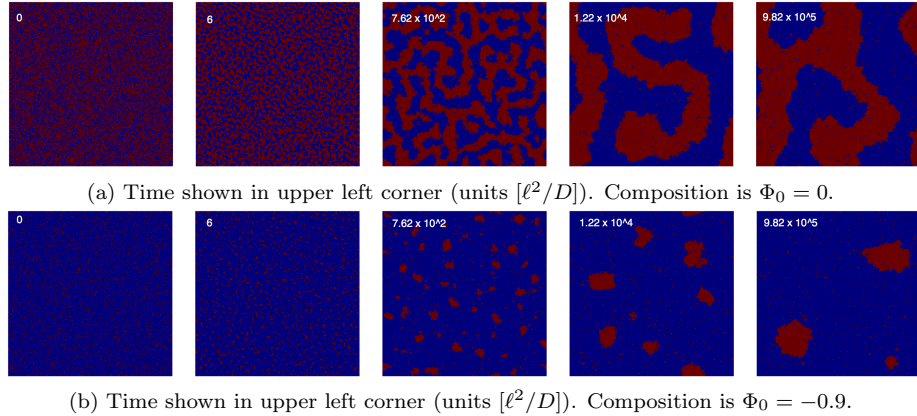


Figure 5.1: Red (Blue) = A (B) type particles. Passive systems with different composition undergoing coarsening. Temperature fixed at  $T/\Omega = 0.4$

two qualitatively different types of coarsening. In systems with even ratios of components we see large, connected regions or “labyrinth patterns” which tend to minimize their interfacial area by forming increasingly rounded shapes. This contrasts with systems which have largely uneven compositions, in which “droplets” quickly form rounded shapes which minimize their own surface area. The system then coarsens by allowing some, usually larger, droplets to grow at the expense of others, which decreases the total interfacial area of the system.

To explore the effect of temperature and composition on the growth dynamics in a more quantitative way we looked at the evolution of the mean wavenumber  $\langle q \rangle(t)$  from the structure factor through time. We expect  $\langle q \rangle$  to decrease with time in systems which undergo coarsening, eventually reaching a steady state value in finite size systems. When the system is near the critical temperature this steady-state value is sensitive to changes in both temperature and composition. However, when we are far from the critical temperature ( $T/\Omega < 0.5$   $T/\Omega > 20$ , data not shown)  $\langle q \rangle$  collapses to a single value. This value is unaffected by small changes in temperature or composition. In figures 5.2 and 5.3 we show  $\langle q \rangle(t)$  over a range of temperatures for two different compositions  $\Phi = 0, -0.9$ .

We see in figure 5.2 that increasing the temperature decreases the rate of coarsening as well as increasing the steady-state value of  $\langle q \rangle$ . Fluctuations are strongly reduced for the lowest temperature  $T/\Omega = 0.45$ , which is the point of total phase separation for all  $\Phi_0$  (see figure 4.3). System at  $T/\Omega = 0.45$  exhibits power-law domain growth similar to  $\langle q \rangle \propto t^\alpha$  with  $\alpha = -0.34$ . This is comparable with the exponent  $\alpha = -1/3$  predicted by standard Lifshitz-Slyozov growth [13].

We see in figure 5.3 that the temperature has a stronger affect on growth rate when the system has an uneven composition, as compared with the  $\Phi_0 = 0$  system shown in figure 5.2. Fluctuations are visibly increased in comparison

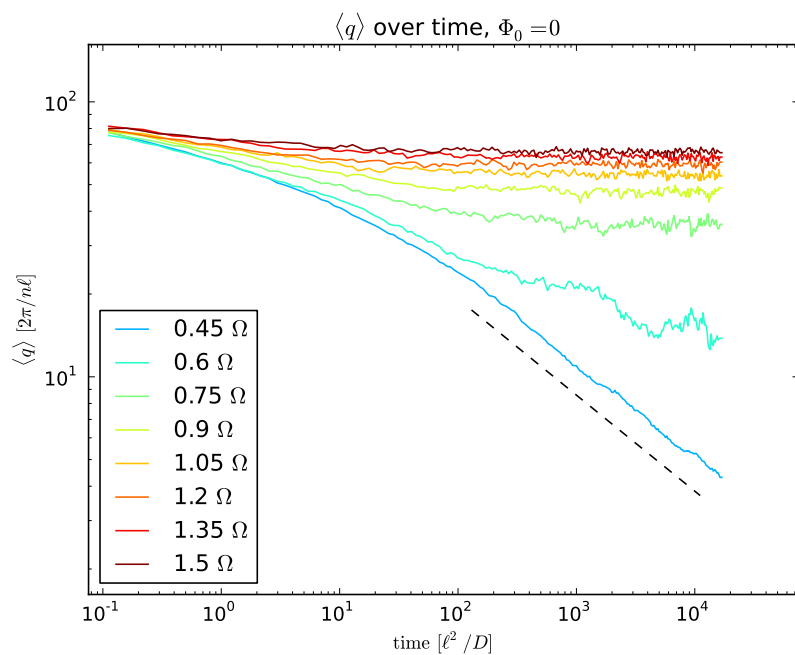


Figure 5.2: Log-log plot of mean wavenumber  $\langle q \rangle$  as a function of time in a passive system with  $\Phi_0 = 0$ . Warmer colors show higher temperature. Dashed black line has slope -0.34.

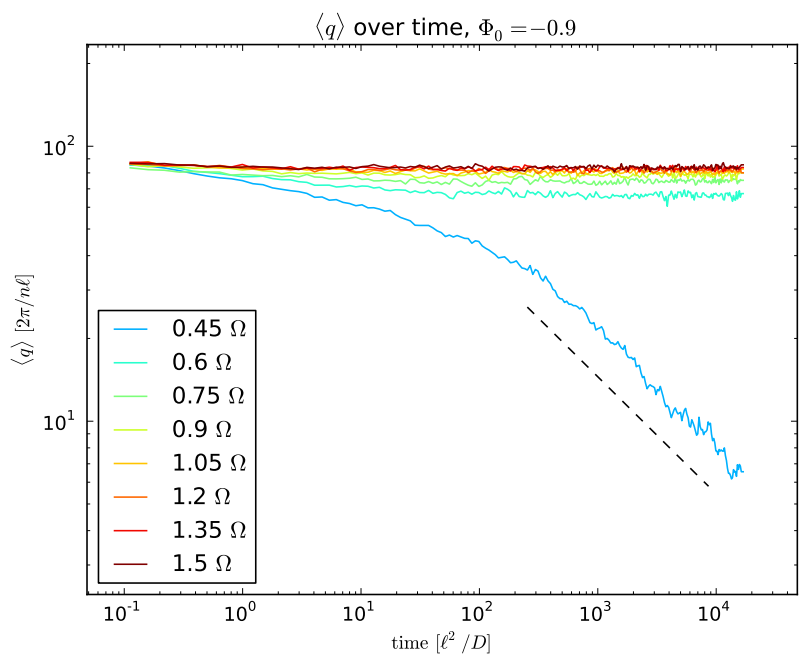


Figure 5.3: Log-log plot of mean wavenumber  $\langle q \rangle$  as a function of time in a passive system with  $\Phi_0 = -0.9$ . Warmer colors show higher temperature. Dashed black line has slope -0.40.

with  $\Phi = 0$  system. Additionally in figure 5.3 power-law growth of domains  $\langle q \rangle \propto t^\alpha$  is observed with  $\alpha \approx -0.40$ .

## 5.2 First order reactions

In systems with first order chemical reactions  $A \leftrightarrow B$  the desire to organize into domains of constant phase fights against the mixing caused by chemical turnover. The introduction of these rates determines a limit to the coarsening and allows patterns of finite wavelength to persist in steady state (figs. 4.5, 4.4).

In this section we explore the dynamic effects of these reactions on the structure factor mean  $\langle q \rangle(t)$ . To do this we ran simulations for a wide range  $-4 < \log_{10} \Gamma_1 < 6$  of values of the symmetric rate  $\Gamma_1 = k_{BA} + k_{AB}$ .

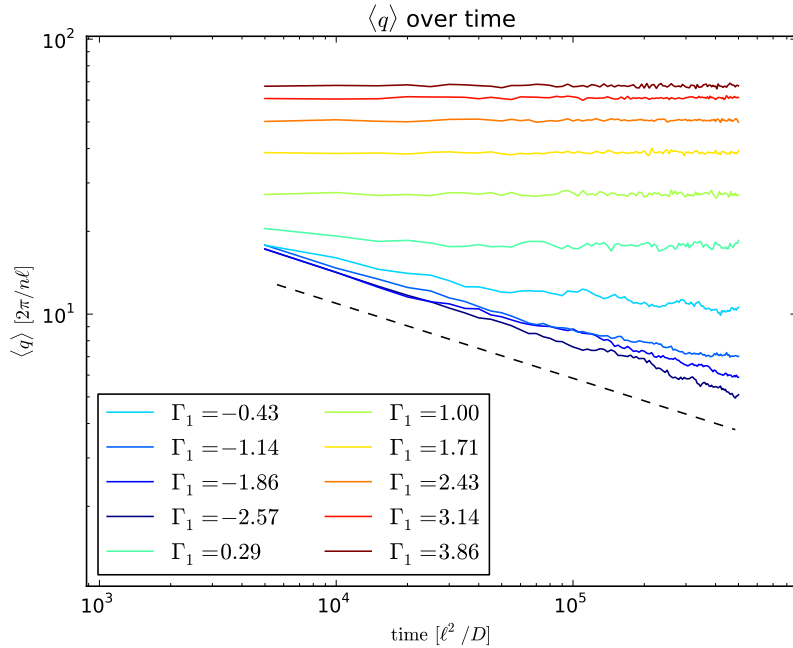


Figure 5.4: Log-log plot of mean wavenumber  $\langle q \rangle$  as a function of time in an active system with first-order chemical reactions. Asymmetric rate  $\Gamma_2 = 0$ . Warmer colors show higher symmetric rate  $\Gamma_1 [D/2n^2\ell^2]$ . Temperature  $T/\Omega = 0.5$ . Dashed black line has slope -0.27.

We see in figure 5.4 that a steady state  $\langle q \rangle$  is reached more quickly by systems with higher  $\Gamma_1$ . We also observe a power-law behavior  $\langle q \rangle(t) \propto t^\alpha$  with  $\alpha \approx -0.27$  in all systems with  $\Gamma_1 < 10^{-1}$ , small enough that coarsening could be observed for significant time. This is a significant deviation from the exponent

$\alpha = -0.34$  in passive systems with the same composition, but may be the result of the competition between the effective pushing and pulling forces introduced at the beginning of the chapter.

### 5.3 Autocatalytic reactions

In autocatalytic systems we see the same competition that is observed in first order systems between coarsening due to phase separation and mixing due to chemical reactions. Additionally, it is already apparent from Landau theory that the behavior of the composition  $\Phi(t)$  can no longer be treated separately from the morphology. The nonlinearities introduced by autocatalysis in the continuous equations (3.34) prevent us from decoupling the evolution of the average composition  $\Phi(t)$  from the local composition  $\phi(\mathbf{x}, t)$ .

To investigate the effects on the composition we simulated the lattice with autocatalytic reactions for a range of values of the reaction rates  $k_q$  and  $k_{BA}$ . In figure 5.5 we plot  $\Phi(t)$  from simulations of the lattice model with autocatalytic reactions. The individual rates  $k_q$  and  $k_{BA}$  are varied, but their ratio is fixed  $k_q/k_{BA} = 2$ . We can see that  $\Phi(t)$  exhibits non-monotonic behavior at early times for a range of reaction rates near  $k_{BA} = 10^{-1} [D/2n^2\ell^2]$ . Initially the system is well mixed which allows the autocatalytic reaction to drive the composition to a state of predominantly B particles. As the system coarsens the interfacial area decreases and the autocatalytic reactions slow down, allowing the first order rate  $k_{BA}$  to drive the system back to a state of predominantly A particles.

We have also briefly explored the dynamics of domain growth in autocatalytic systems through analysis of the mean wavenumber  $\langle q \rangle$  from the structure factor (3.4). In figure 5.6 we show  $\langle q \rangle$  over time on a double-logarithmic scale for different values of the autocatalytic reaction rate  $k_q$ . The first-order back rate is fixed  $k_{BA} = 1$ . We see power-law coarsening independent of  $k_q$  of the form  $\langle q \rangle \propto t^\alpha$  where  $\alpha = -0.20$ . This rate is lower than both the coarsening exponent found in passive systems with  $\Phi = 0$  of  $\alpha = -0.34$  and the exponent found in active systems with first-order chemical reactions  $\alpha = -0.27$ .

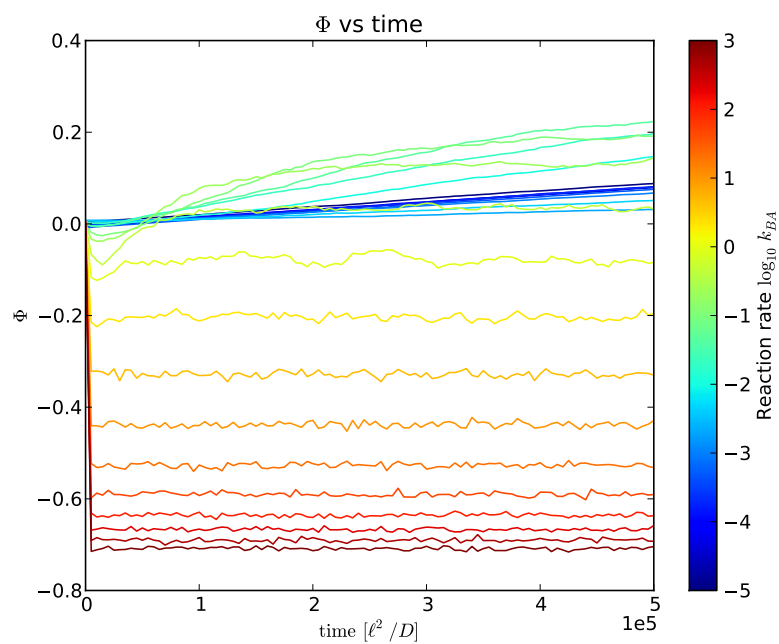


Figure 5.5: Composition  $\Phi$  over time in an autocatalytic system. Warmer colors show higher reaction rate ( $\log_{10}$  scale)  $k_{BA}$  with units  $[D/2n^2\ell^2]$ . Temperature fixed at  $T/\Omega = 0.5$ . The ratio  $k_q/k_{BA} = 2.0$  is also fixed.

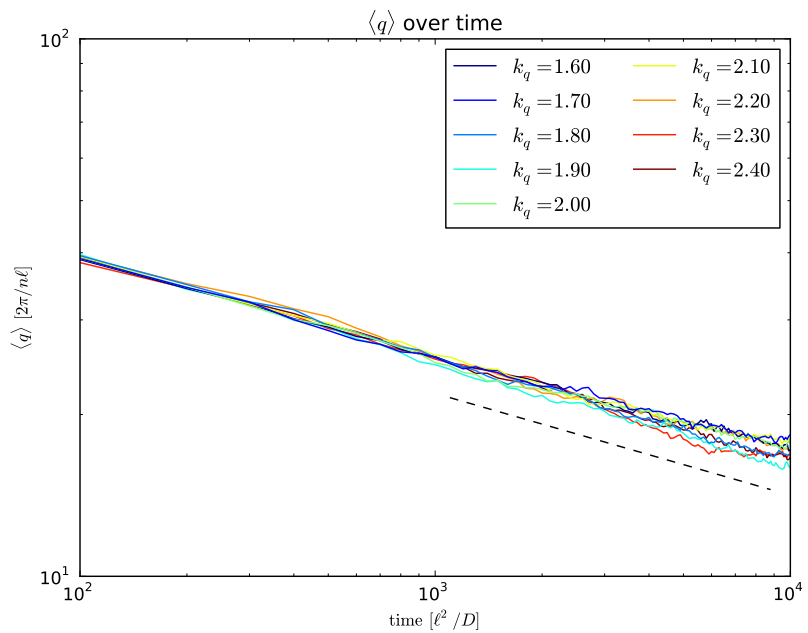


Figure 5.6: Log-log plot of mean wavenumber  $\langle q \rangle$  as a function of time in an active system with autocatalytic reactions. First order back rate fixed:  $k_B A = 1$ . Warmer colors show higher autocatalytic rate  $k_q [D/2n^2\ell^2]$ . Temperature fixed at  $T/\Omega = 0.5$ . Dashed black line has slope -0.19.

# Chapter 6

## Summary

In this thesis we studied the properties of isotropic, binary mixtures undergoing phase separation in chemically reactive fluid. The introduction of chemical reactions into the description of coarsening leads to range of interesting behavior.

### 6.1 Steady state behavior

In systems at low temperature  $T/\Omega < 0.45$  we see sharper lines between regions of differing phase. Domains exhibit rounded morphologies. As we increase the temperature  $T/\Omega > 0.45$  the interface between domains begins to blur noticeably as the entropic effects become more important. In passive systems we observe a continuous transition in  $\langle q \rangle$  over a range of temperatures near the critical temperature predicted by mean-field theory  $T_c = \Omega$  (eq. 3.22). At scaled temperatures  $T/\Omega < 0.45$  and  $T/\Omega > 10$  the mean wavenumber  $\langle q \rangle$  collapses to a single value. The phase behavior of the system in these regions is insensitive to changes in either temperature or composition. Passive systems coarsen indefinitely, as no competing mechanism exists to counter phase separation. The characteristic scale of structures in steady state is only limited by the size of the system and the amount of material. In phase separating systems with actively driven first-order chemical reactions of the form



we observe patterns of a finite characteristic scale which persist in steady state. This characteristic length scale in decreased as we increase the rate of chemical reactions. The average composition of these systems is determined completely by the chemical reaction rates, and takes on a value in steady of  $\Phi = \frac{k_{BA} - k_{AB}}{k_{BA} + k_{AB}}$ .

In systems with the actively driven chemical reactions



we observe a dependence of the total speed of reactions on the system’s morphology in addition to the domain size scaling seen in first order systems. In phase separating systems autocatalytic reactions are driven more strongly when the total interfacial area between phases is greater. This leads to a complex dependence of the steady state composition on both the reaction rates  $k_q$  and  $k_{BA}$  and the scaled temperature  $T/\Omega$ .

## 6.2 Coarsening dynamics

In both passive and active systems we observe coarsening dynamics which tend to minimize the interfacial area between phases. At scaled temperatures below  $T/\Omega = 0.45$  two qualitatively different coarsening patterns exist. Systems with more even amounts of A and B particles form “labyrinth patterns” which minimize the total interfacial area by changing the shape of domains to make them more round. Systems where one particle type dominates form a large number of round “droplets”. The system minimizes its interfacial area by allowing some (usually larger) droplets to grow while others dissolve. In all systems the growth of the characteristic size of domains seems to increase until a maximum growth rate is reached, at which point it follows a power law. The scaling exponent decreases when chemical reactions are introduced, leading to slower coarsening rates. We interpret this slowing down as a competition between short range attractive forces and an effective long range pushing force between regions of similar phase. In passive systems we observe power-law coarsening which is not inconsistent with classical Lifshitz-Slyozov behavior. In active systems with either first order or autocatalytic chemical reactions we see smaller exponents  $\alpha$  indicating slower coarsening rates. Additionally in active systems non-monotonic behavior of the composition  $\Phi(t)$  over time is observed as a result of the interplay between system morphology and the autocatalytic reactions.

## 6.3 Outlook

- One of the most interesting prospects for this work is the ability to study the effect of chemical reactions on the scaling exponents  $\alpha$ . To do this in a quantitative way does not require any modifications to the simulation algorithms, but only a significant amount of computational time.
- Allowing for an effective “polymerization” between adjacent components as described by the Flory-Huggins model may be able to extend the relevance of our simulations to descriptions of gels, which exhibit a wide variety of phase behavior.
- Clearly, the complexity of behavior available in systems of this type is limited in part by the number of components. While many physical systems can be successfully modeled as consisting of only two components,

extending this model to three or greater may introduce rich new types of behavior.



# Bibliography

- [1] JG Amar, FE Sullivan, and RD Mountain. Monte Carlo study of growth in the two-dimensional spin-exchange kinetic Ising model. *Physical Review B*, 37(1), 1988.
- [2] F S Bates. Polymer-polymer phase behavior. *Science*, 251(4996):898–905, 1991.
- [3] Kurt Binder and DW Heermann. *Monte Carlo Simulation in Statistical Physics*. 2010.
- [4] Clifford P Brangwynne, Timothy J Mitchison, and Anthony a Hyman. Active liquid-like behavior of nucleoli determines their size and shape in *Xenopus laevis* oocytes. *Proceedings of the National Academy of Sciences of the United States of America*, 108(11):4334–9, March 2011.
- [5] John W. Cahn. Phase Separation by Spinodal Decomposition in Isotropic Systems. *The Journal of Chemical Physics*, 42(1):93, 1965.
- [6] M E Cates, D Marenduzzo, I Pagonabarraga, and J Tailleur. Arrested phase separation in reproducing bacteria creates a generic route to pattern formation. *Proceedings of the National Academy of Sciences of the United States of America*, 107(26):11715–20, June 2010.
- [7] PM Chaikin and TC Lubensky. *Principles Of Condensed Matter Physics*. 2000.
- [8] Jacob J Christensen, Ken Elder, and Hans C Fogedby. Phase segregation dynamics of a chemically reactive binary mixture. 54(3):2212–2215, 1996.
- [9] SC Glotzer and Wolfgang Paul. Molecular and mesoscale simulation methods for polymer materials. *Annual Review of Materials Research*, 32(1):401–436, August 2002.
- [10] SC Glotzer, D Stauffer, and Naeem Jan. Monte Carlo simulations of phase separation in chemically reactive binary mixtures. *Physical review letters*, 72(26):4109–4113, 1994.
- [11] JS Langer. Theory of spinodal decomposition in alloys. *Annals of Physics*, 5346, 1971.

- [12] Chiu Fan Lee, Clifford P. Brangwynne, Jöbin Gharakhani, Anthony a. Hyman, and Frank Jülicher. Spatial Organization of the Cell Cytoplasm by Position-Dependent Phase Separation. *Physical Review Letters*, 111(8):088101, August 2013.
- [13] IM Lifshitz and VV Slyozov. The kinetics of precipitation from supersaturated solid solutions. *Journal of Physics and Chemistry of Solids*, 19(1):35–50, 1961.
- [14] Fong Liu and N Goldenfeld. dynamics of phase separation in block copolymer melts. *Physical Review A*, 39(9):4805–4810, 1989.
- [15] Quan-Xing Liu, Arjen Doelman, Vivi Rottschäfer, Monique de Jager, Peter M J Herman, Max Rietkerk, and Johan van de Koppel. Phase separation explains a new class of self-organized spatial patterns in ecological systems. *Proceedings of the National Academy of Sciences of the United States of America*, 110(29):11905–10, July 2013.
- [16] Amy Novick-Cohen and LA Segel. Nonlinear aspects of the Cahn-Hilliard equation. *Physica D: Nonlinear Phenomena*, pages 277–298, 1984.
- [17] CS Shida and VB Henriques. Kawasaki dynamics and equilibrium distributions in simulations of phase separating systems. *arXiv preprint cond-mat/9703198*, page 6, March 1997.